Setup and Characterization of a High-Dynamic-Range Third-Order Correlator for 1 kHz laser system

DIPLOMARBEIT

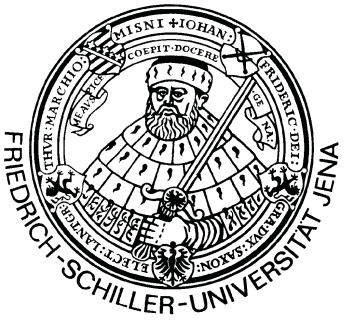

FRIEDRICH-SCHILLER-UNIVERSITÄT JENA

PHYSIKALISCHE-ASTRONOMISCHE FAKULTÄT

Jena, August 2004

eingereicht von: Nguyen Xuan Truong

geb. am: 09.08.78 in Haiduong - Vietnam

1. Evaluator: ....

2. Evaluator: ....

Date of lending out: ....

Contents

List of Figures

List of Tables

Chapter 1

Introduction

Since the invention of the laser in 1960 with the work of Maiman [1], the laser pulse duration has been dramatically reduced through the development of various techniques such as Q-switching and mode-locking [2]. In 1981, after two decades of extensive research and innovation, the first laser pulse in subpicosecond region had been successfully generated [3], initiating the revolution of ultrashort (< 1 ps) laser pulse generation. Nowadays, with the discovery of the passive mode-locking based on the nonlinear Kerr effect in the active material (Ti:sapphire), the shortest-generated laser pulse duration of about 5 fs have been recently reported [4, 5]. The ultrashort laser pulses have then become an important tool to study ultra-fast phenomena and to generate compact extremely high-intensity laser pulses. The decisive breakthrough was the introduction of Chirped Pulse Amplification (CPA) technique [6], making possible the generation of laser pulses in the laboratory with intensity up to 10^{21} Wcm^{-2} [7]. Such ultrashort ultrahigh-intensity laser pulses are needed for a variety of research fields, for instance: the study of multi-photon ionization [8], high-harmonic generation [9], laser-matter interaction [10, 11], and the laser-induced nuclear physics [12]. Despite the fact that the oscillators can produce high-contrast ultrashort laser pulses [13, 14], the chirped pulse amplifiers may generate high-energy laser pulses with a pedestal (for instance, Amplified Spontaneous Emission (ASE)) temporally extending much longer than the pulse duration.

In laser-matter interaction experiments, a high-peak power short pulse must usually interact directly with a solid target, which can be seriously damaged or even vaporized with an intensity of about $10^{10} - 10^{12}$ Wcm^{-2} (depending on target material and pulse duration). Hence, when a laser beam with focused intensity 10^{17} Wcm^{-2} reaches the target, it is important to monitor the pre-pulses and pedestals with intensities less than 10^{-7} of the peak intensity. If, however, the pre-pulses or pedestals come with intensities above the threshold, they will create a large preformed plasma before the arrival of the main pulse. Many experiments studying the influence of

the preformed plasma have been reported. Measuring the preformed plasma from a plastic foil target, Giulietti *et al.* [15] realized the significant influence of preformed plasma on the production of collimated electrons. By elongating the rise-time of the X-ray pulse, the preformed plasma prevents the creation of the population inversion, as reported in [16,17]. In addition, the preformed plasmas also affect the propagation of the main pulse, for example, through the channel formation processes discussed in [18, 19, 20]. In X-ray experiments, which are of interest in our present projects, it has been shown that the X-ray yield is increased if the laser pulse interacts *not with the surface of the solid target but with a preformed plasma* generated by a pre-pulse or a pedestal from the laser [21]. Therefore, detailed knowledge of the pulse shape and contrast ratio is essential for experiments of ultrashort ultrahigh-intensity laser-matter interactions.

The contrast[1] ratio here implies a measure of how far in time and intensity the main pulse can be considered to be free of pre- and post-pulses as well as the level of pedestals. For ultrahigh-intensity laser pulses, the High-Dynamic-Range measurements of optical pulse are therefore of great interest. In principle, such a measurement must be fulfilled over nanosecond range to yield an entire history of the laser pulse[2]. In the near infrared region, the contrast measurements using second-harmonic and third-harmonic generation or plasma-shuttered streak camera have been already realized.

Being the first autocorrelation technique invented to characterize the ultrashort laser pulse, second-order autocorrelator is usually used for its simple implementation. Because of second-harmonic generated by scattering of either of the two input beams on the surface of nonlinear crystal, the second-order autocorrelator is, however, limited by the dynamic range of about 10^5 and can be increased to about two additional orders of magnitude by applying the chopper-technique [14, 22]. It, however, shows ambiguity in time-direction.

To overcome the problem of time-direction ambiguity, the high-order correlation techniques have been considered [23, 24, 25]. It has been proven that it is enough to determine the pulse shape with third-order correlation technique. Applying third-harmonic generation with combination of two nonlinear crystals, S. Luan and coworkers [25] realized a high-dynamic range of about 10^8. The experiments with third-order correlators show simple implementation, high contrast and reliable pulse asymmetry measurement.

[1] Throughout this work, the contrast of a structure is assumed to be the ratio of the peak intensity of the pulse to the intensity of this structure while the intensity of a structure is the inverse of its contrast.

[2] For many cases, a temporally long (nanosecond) pedestal may have a significant percentage of laser energy.

Because of the requirement of the physical overlap[3] of the interacting pulses in nonlinear crystals, the practical disadvantage of using the correlation technique is that its temporal range is just around the main pulse (several hundred picoseconds). Streak cameras allow one to measure over a long time duration but have a low-dynamic range of about 100, while the required dynamic range is usually of about $10^6 - 10^8$. To be able to measure the pedestals without damaging the streak camera, a mechanism could be applied, which lets the pedestal through and simultaneously attenuates the main pulse. Such a technique has been developed in the work of Tien *et. al* [26] by combining a plasma shutter and a multi-shot averaging implemented with photoconductive switch sweep circuit. This technique has been used successfully to measure the contrast of ultrashort laser pulse over 2 ns with 10^7 dynamic range. The time-resolution of the streak camera, however, of $\sim$ 1 ps and hence the technique can not be applied to measure the pulse duration in the femtosecond range. Depending on the requirements of appropriate experiments in the laboratory, the technique using correlation *and/or* plasma shutter with streak camera should be chosen.
The purpose of this work is to build and characterize a high-dynamic-range third-order correlator used to characterize the 1 kHz-laser system for laser-matter interaction experiments. With the focused intensity reaching 10^{17} Wcm^{-2}, it is required for the correlator to realize a high dynamic range of more than 7 orders of magnitude. The experimental setup is principally similar to that discussed in [25] and is theoretically expected to reach $\sim 10^{11}$ high-dynamic range. The work is mainly structured as follows:

- *Chapter 1* introduces briefly the necessity and the requirements of a high-dynamic range third-order correlator.
- *Chapter 2* discusses the background information about the ultrashort laser pulses such as the generation and description of ultrashort laser pulses, and the correlation technique exploiting nonlinear optics, which are very important to understand, implement the experiments, and analyze the measured data.
- *Chapter 3* describes the principles and experimental setup of the high-dynamic range third-order correlator. The 1kHz-laser system used to experiment is also briefly discussed in this chapter.
- *Chapter 4* presents the experimental results and respective analysis for characterizing the high-dynamic range third order correlator.

[3] "Physical overlap" means temporal and spatial overlap.

Chapter 2

Fundamentals of Ultrashort Laser Pulses

2.1 Generation of ultrashort laser pulses

To generate optical pulses in the femtosecond regime one needs a bandwidth of more than 1 THz, a suitable active medium-which is able to amplify this bandwidth, and a mechanism to couple all of the modes (mode-locking technique, see for example [2]). To date, many different laser mode-locking techniques have been developed, but all have to provide two basic functions: forcing all the modes to be equally spaced and to have the same phase at one instant of time. Normally, these requirements can be achieved with help of an external modulation (active mode-locking) or a saturable absorbing medium (passive mode-locking). However, in some types of laser materials, the modes may be able to lock themselves, partially or totally, in the active medium. One of the most common techniques for generating ultrashort laser pulses is the passive mode-locking of Ti:sapphire (Ti:Al_2O_3) lasers based on the nonlinear Kerr effect. In such a laser material, the laser waves with stronger peak intensities experience less losses, and thus will be selectively modified with respect to intensity.

Considered as the laser material with optimal properties, the Ti:Al_2O_3 crystal produces gain stretching from 650 nm to 1100 nm [27], what is equivalent to a bandwidth of 200 THz and a shortest-possible pulse duration of ~ 4 fs. It also has a very high thermal conductivity, a relatively large emission cross section ($\sim 3 \cdot 10^{-19}$ cm^2 at 800 nm), as well as a saturation flux density of about 1 J/cm^2. Because the Kerr effect of this crystal is instantaneous and not dependent on the stored energy density, it enables a totally new class of laser systems with good beam quality and extremely high powers. While the mode-locking process can be described relatively easily in the frequency-domain [28], a truly successful, comprehensive, and quantitative the-

ory for ultrashort lasers is still not possible. Therefore, the generation of ultrashort laser pulses of Ti:Al_2O_3 will be only qualitatively discussed.
A typical cavity design of a Ti:Al_2O_3 oscillator using the Kerr lens mode-locking is shown in Fig. 2.1 [28]. The Ti:Al_2O_3 crystal is found in the focus of the two mirrors. The dichroic mirror M_2 is highly transparent at the wavelength of the pump laser (usually about 0.53 μm) and reflects at about 0.8 μm, which is the central emission wavelength of Ti:Al_2O_3 laser.

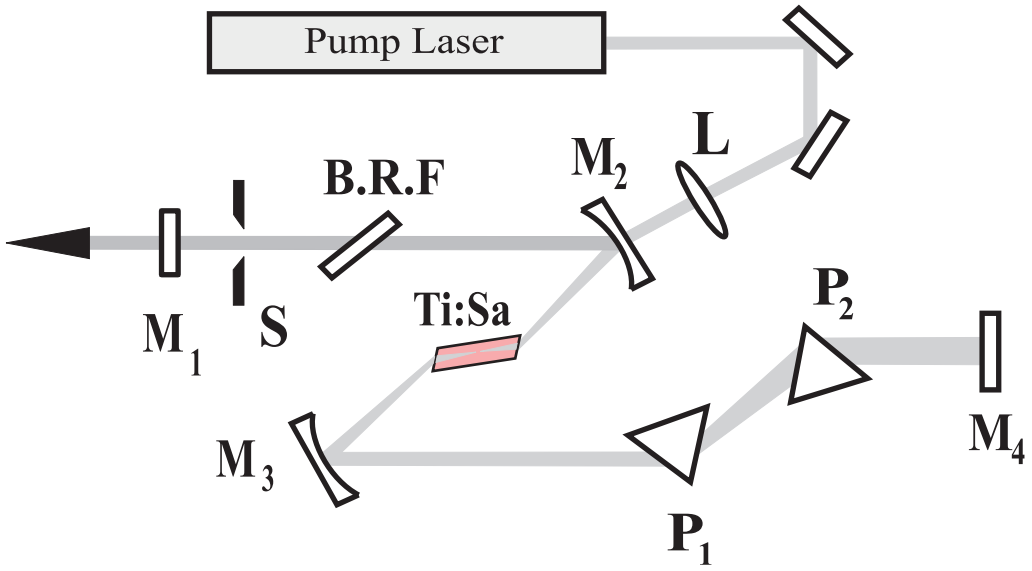

Fig. 2.1: Schema of a self-mode-locked Ti:sapphire laser using the Kerr lens mode-locking process.

When passing through the Ti:Al_2O_3 crystal, a wave with, for instance, a Gaussian profile feels an inhomogeneous refractive index because of its intensity dependence: $n = n_0 + n_2 I(\vec{r}, t)$, n_2 is of the order of 10^{-16} cm^2/W. As shown later in the section of nonlinear optics, the crystal behaves like a converging lens and focuses the laser beam. The oscillator must be so designed that the losses are larger without the appearance of this lens. This explains for the presence of the adjustable slit S in Fig. 2.1.
The central wavelength of the laser system can be changed by turning the birefringent filter (B.R.F). Because the Ti:Al_2O_3 crystal shows positive dispersion in near infra-red region, simple chirp compensation in the resonator, for instance, using the two prisms as shown in Fig. 2.1, is required. Special dielectric mirrors, called chirp-compensating mirrors, have also been used for the compensation of linear and nonlinear dispersion. By these mirrors, the different wavelengths are effectively reflected at different depths and thus have different optical delays in the sub-μm range. In addition, the refractive index of the active medium varies as a function of

time, and thus causes the self-phase modulation. This effect broadens the spectrum and thereby introduces further shortening of the pulses. By using the compensation techniques discussed above the shortest pulse generated with Ti:Al_2O_3 lasers has been recently reported [4, 5], which has duration of ~ 5 fs and contains only ~ 2.7 optical cycles at FWHM.

2.2 Theoretical Description

2.2.1 Complex Representation

Electromagnetic waves can be completely described by the time and space dependent electric field vector, which is a real quantity and may be directly measured in three dimensions [29]. However, it is sometime more convenient for theoretical descriptions to write the electric field vector in complex form, especially in dealing with propagation problems of electromagnetic pulses. In the absence of the sources of the fields, the Maxwell equations in an infinite medium are [30]:

$$\nabla \times \tilde{\mathbf{E}} = -\frac{\partial \tilde{\mathbf{B}}}{\partial t} \tag{2.1}$$

$$\nabla \times \tilde{\mathbf{H}} = \frac{\partial \tilde{\mathbf{D}}}{\partial t} \tag{2.2}$$

$$\nabla \cdot \tilde{\mathbf{D}} = 0 \tag{2.3}$$

$$\nabla \cdot \tilde{\mathbf{B}} = 0 \tag{2.4}$$

and the material equations

$$\tilde{\mathbf{D}} = \epsilon_0 \tilde{\mathbf{E}} + \tilde{\mathbf{P}} \tag{2.5}$$

$$\tilde{\mathbf{B}} = \mu_0(\tilde{\mathbf{H}} + \tilde{\mathbf{M}}), \tag{2.6}$$

where

$\tilde{\mathbf{E}}$:	the electric field	$\tilde{\mathbf{H}}$:	the magnetic field
$\tilde{\mathbf{D}}$:	the electric displacement	$\tilde{\mathbf{B}}$:	the magnetic induction
$\tilde{\mathbf{P}}$:	the polarization vector	$\tilde{\mathbf{M}}$:	the magnetization vector
ϵ_0:	the dielectric constant of vacuum	μ_0:	the permeability of vacuum.

The polarization vector $\tilde{\mathbf{P}}$ describes the field-material interaction and generally depends upon the electric field $\tilde{\mathbf{E}}$ in the form [31]:

$$\begin{aligned}\tilde{\mathbf{P}} = \quad & \epsilon_0\underline{\chi}^{(1)} : \tilde{\mathbf{E}} \quad && \text{the linear polarization} \\ + \quad & \epsilon_0\underline{\chi}^{(2)} : \tilde{\mathbf{E}}^2 && \text{the second-order nonlinear polarization} \\ + \quad & \epsilon_0\underline{\chi}^{(3)} : \tilde{\mathbf{E}}^3 && \text{the third-order nonlinear polarization} \\ + \quad & \cdots && \cdots\end{aligned} \tag{2.7}$$

Here the i-order susceptibility $\underline{\chi}^{(i)}$ are the $(i+1)$-order tensors determined by the symmetry properties of the nonlinear medium.
In the case of a linear, isotropic, homogenous medium, the material equations are written as:

$$\tilde{\mathbf{D}} = \epsilon\epsilon_0\tilde{\mathbf{E}} \qquad \text{and} \quad \tilde{\mathbf{B}} = \mu\mu_0\tilde{\mathbf{H}}, \tag{2.8}$$

where ϵ and μ are the relative dielectric constant and the relative permeability, respectively. Introducing Eq.(2.8) into the Maxwell equations, we obtain the homogenous wave equations for the electric field:

$$\nabla^2\tilde{\mathbf{E}} - \frac{1}{v_p^2}\frac{\partial^2\tilde{\mathbf{E}}}{\partial t^2} = 0, \tag{2.9}$$

where $v_p = 1/\sqrt{\epsilon\epsilon_0\mu\mu_0} = c/n$ and $n = \sqrt{\epsilon\mu}$ is called the refractive index of the medium. For reason of simplification, we consider the solution of a monochromatic planar light wave, which is linearly polarized and propagates in the z-direction with frequency ν:

$$\mathrm{E}_e(z,t) = E_0\cos[2\pi\nu t - kz + \varphi_0] = \Re e\{E_0 e^{i[2\pi\nu - kz + \varphi_0]}\}, \tag{2.10}$$

where E_0 is the amplitude, φ_0 is the initial phase, and $k = k(\nu) = 2\pi\nu n/c$ is the wave number.
To avoid the complicated algebra of trigonometric functions, here and in what follows, we will use the complex representation and note that only the real part of this expression describes the electric field. Because of the linearity of Eq.(2.9), the general solution can be obtained by taking the linear combination of every possible solution (2.10):

$$\begin{aligned}\tilde{\mathrm{E}}(z,t) &= \int_0^\infty E_0 e^{i[2\pi\nu t - kz + \varphi_0]}d\nu \\ &= \frac{1}{2\pi}\int_0^\infty \tilde{E}(z,\omega)e^{i\omega t}d\omega\end{aligned} \tag{2.11}$$

The electric field can be described more elegantly by using the Fourier-Transformation. In order to do that, we assume

$$\tilde{E}(\omega) = 0 \qquad \text{for} \quad \omega < 0. \tag{2.12}$$

Now, neglecting the spatial dependence, we can express the relationships between the temporal electric field and its spectrum as[1]:

$$\tilde{\mathrm{E}}(t) = \frac{1}{2\pi} \int \tilde{E}(\omega) e^{i\omega t} d\omega \tag{2.13}$$

and

$$\tilde{E}(\omega) = \int \tilde{\mathrm{E}}(t) e^{-i\omega t} dt. \tag{2.14}$$

The real electric field can be then derived from the complex quantity by

$$\mathrm{E}(t) = \tilde{\mathrm{E}}(t) + \text{c.c.}, \tag{2.15}$$

where c.c. stands for **c**omplex **c**onjugate.
In most practical cases of interest, the spectral amplitude will be centered around a mean frequency ω_l and will have appreciable values only in a frequency interval $\triangle\omega$ small compared to ω_l. As a result, in the time domain, the complex electric field can be separated into an amplitude function, which varies slowly with time, and a phase term, which changes with carrier frequency ω_l:

$$\tilde{\mathrm{E}}(t) = A(t) e^{i\varphi(t)} e^{i\omega_l t} = \tilde{A}(t) e^{i\omega_l t}, \tag{2.16}$$

where $A(t)$ is called the field envelope, $\tilde{A}(t)$ the complex field envelope, and $\varphi(t)$ is the time dependent phase, respectively. The definition of the concept of an envelope and carrier frequency makes sense in the cases where the bandwidth is only a small fraction of the carrier frequency, namely:

$$\frac{\triangle\omega}{\omega_l} \ll 1. \tag{2.17}$$

This treatment is also called the **S***lowly* **V***arying* **E***nvelope* **A***pproximation* (SVEA)[2]
It is obvious from Eq.(2.16) that the choice of carrier frequency and phase $\varphi(t)$ is not unique. The most useful choice of carrier frequency should be one that ensures the minimum variation of phase during the intense portion of the pulse. For practical reasons, the carrier frequency at the pulse peak is usually the choice. In general a

[1] In this work we imply that $\int(\cdots) = \int_{-\infty}^{\infty}(\cdots)$.

[2] This assumption also implies the neglect of backwards generated waves [32] in nonlinear optics, which is referred to later.

better definition, which is consistent in the time and frequency domains, is to use the intensity weighted average frequency:

$$\omega_l = \frac{\int |\tilde{\mathrm{E}}(t)|^2 \omega(t) dt}{\int |\tilde{\mathrm{E}}(t)|^2 dt} = \frac{\int |\tilde{E}(\omega)|^2 \omega d\omega}{\int |\tilde{E}(\omega)|^2 d\omega} \tag{2.18}$$

The intensity is defined as the instantaneous pulse power per unit area [W/cm^2] and reads:

$$\begin{aligned} I(t) &= \epsilon_0 cn \frac{1}{T} \int_{t-T/2}^{t+T/2} \mathrm{E}^2(t') dt' \\ &= 2\epsilon_0 cn A^2(t) = 2\epsilon_0 cn |\tilde{A}(t)|^2, \end{aligned} \tag{2.19}$$

where $T = 2\pi/\omega_l$ is the optical period. From the experimental point of view, T has to be replaced by the actual response time of the detector. The spectral intensity can be obtained with help of the Parseval's theorem [33]:

$$S(\omega) = \frac{\epsilon_0 cn}{\pi} |\tilde{E}(\omega)|^2. \tag{2.20}$$

2.2.2 Pulse duration and spectral width

It is difficult to assert the detailed characteristics of light pulse when its duration becomes shorter and shorter. Part of the problem is how to define the pulse duration and the spectral width so that they can give possibly exact information of the considered pulse, especially in the femtosecond domain-where nowadays the shortest-generated laser pulses contain only a few optical cycles. The standard statistical definitions are usually used in theoretic calculations and given as:

$$\tau_p^2 = \frac{\int (t - t_p)^2 |\tilde{\mathrm{E}}(t)|^2 dt}{\int |\tilde{\mathrm{E}}(t)|^2 dt} \tag{2.21}$$

$$\triangle\omega_p^2 = \frac{\int (\omega - \omega_p)^2 |\tilde{E}(\omega)|^2 d\omega}{\int |\tilde{E}(\omega)|^2 d\omega}, \tag{2.22}$$

where t_p is the intensity weighted average time [defined similarly to (2.18)]. With help of the Schwarz's inequality [34], one can show that these quantities are related through the following universal inequality:

$$\triangle\omega_p \tau_p \geq \frac{1}{2}. \tag{2.23}$$

From the relation (2.23), some important conclusions for experiments in the field of ultrashort light pulses can be made:

- In order to produce a ultrashort light pulse with a given duration, one needs to find a active medium, which is able to support a broad enough spectral bandwidth. For instance, a Gaussian-shaped pulse with pulse duration of 100 fs has a minimum spectral bandwidth of 4.41 THz.
- The equality in (2.23) can only be reached with Gaussian time and spectral envelopes and the pulse is then said to be a Fourier-transform-limited or unchirped pulse. In this case, the instantaneous frequency, defined as the first time-derivative of the phase factor $[\omega t + \varphi(t)]$ in (2.16), is a time-independent quantity.
- For a given spectrum, one pulse envelope can be constructed that has the shortest-possible duration.

In practice, however, half-maximum quantities are easier to measure. Therefore, one defines the pulse duration τ_p as the **F**ull **W**idth at **H**alf **M**aximum (FWHM) of the intensity profile and the spectral width $\triangle\omega_p$ as the FWHM of the spectral intensity. The Fourier inequality is then usually given by:

$$\triangle\omega_p\tau_p = 2\pi\triangle\nu\tau_p \geq 2\pi K, \tag{2.24}$$

where K is a numerical constant, depending on the assumed shape of the pulse.

Gaussian pulses

Let us now consider an example of Gaussian pulse, which is most commonly used in ultrashort laser pulse characteristics. The pulse is linearly chirped and represented by:

$$\tilde{A}(t) = A_0 e^{-(1+i\alpha)t^2/\tau_G^2} \qquad \text{with} \qquad \tau_p = \sqrt{2\ln 2}\tau_G. \tag{2.25}$$

The instantaneous frequency is given as:

$$\omega(t) = \omega_l + \frac{d\varphi(t)}{dt} = \omega_l - \frac{2\alpha}{\tau_G^2}t \tag{2.26}$$

As one can see from (2.26), the pulse is down-chirped for a positive chirp parameter α and vice versa. The spectral intensity can be derived by taking the Fourier-transform of (2.25) and using the Eq.(2.20). It also has the Gaussian shape and reads:

$$S(\Omega) = \frac{\epsilon_0 cn A_0^2 \tau_G^2}{\sqrt{1+\alpha^2}} \exp\left\{ - \frac{\Omega^2\tau_G^2}{2(1+\alpha^2)} \right\}, \tag{2.27}$$

where $\Omega = \omega - \omega_l$ and with a FWHM:

$$\triangle\omega_p = (1/\tau_G)\sqrt{8\ln 2(1+\alpha^2)} \tag{2.28}$$

The pulse duration-bandwidth product is now given by:

$$\triangle\nu_p\tau_p = (\triangle\omega_p/2\pi)\tau_p = \frac{2\ln 2}{\pi}\sqrt{1+\alpha^2} \tag{2.29}$$

The presence of chirp results in significant different delays between the spectrally different components of laser pulse causing pulse broadening effect and leading to a duration-bandwidth product exceeding the Fourier limit ($K_G = 2\ln 2/\pi \approx 0.441$) by a factor $\sqrt{1+\alpha^2}$. This conclusion is also true for the statistical definitions of pulse duration and bandwidth given by Eq.(2.21) and (2.22), respectively:

$$\triangle\omega_p^{(s)}\triangle\tau_p^{(s)} = \frac{\sqrt{1+\alpha^2}}{2}. \tag{2.30}$$

2.3 Propagation

2.3.1 The wave equation

The properties of ultrashort laser pulses have been briefly studied in the last section for the simplest case. In this section, we will generally consider these topics in more detail and the propagation of ultrashort laser pulses through a nonlinear medium without free charges and free currents will be discussed .
The medium is assumed to be nonmagnetic, so that:

$$\tilde{\mathbf{B}} = \mu_0\tilde{\mathbf{H}} \tag{2.31}$$

Introducing the material Eqs.(2.5) and (2.31) into the Maxwell's equations again, we obtain the wave equation:

$$\nabla\times\nabla\times\tilde{\mathbf{E}} + \mu_0\frac{\partial^2\tilde{\mathbf{D}}}{\partial t^2} = 0. \tag{2.32}$$

The first term in (2.32) can be written as:

$$\nabla\times\nabla\times\tilde{\mathbf{E}} = \nabla(\nabla\cdot\tilde{\mathbf{E}}) - \nabla^2\tilde{\mathbf{E}}. \tag{2.33}$$

For vanishing gradient in the dielectric constant and hence $\nabla\cdot\tilde{\mathbf{E}} = 0$, we have

$$\nabla\times\nabla\times\tilde{\mathbf{E}} = -\nabla^2\tilde{\mathbf{E}}. \tag{2.34}$$

It is usually convenient to split $\tilde{\mathbf{P}}$ into its linear and nonlinear parts as:

$$\tilde{\mathbf{P}} = \tilde{\mathbf{P}}^{(1)} + \tilde{\mathbf{P}}^{\mathrm{NL}} \tag{2.35}$$

and write:

$$\tilde{\mathbf{D}} = \tilde{\mathbf{D}}^{(1)} + \tilde{\mathbf{P}}^{\mathrm{NL}} \qquad \text{with} \qquad \tilde{\mathbf{D}}^{(1)} = \epsilon_0 \tilde{\mathbf{E}} + \tilde{\mathbf{P}}^{(1)}. \tag{2.36}$$

Here $\tilde{\mathbf{P}}^{(1)}$ is the linear polarization vector, depending linearly upon the electric field $\tilde{\mathbf{E}}$. In terms of these quantities, the wave equation (2.32) becomes:

$$\nabla^2 \tilde{\mathbf{E}} - \mu_0 \frac{\partial^2 \tilde{\mathbf{D}}^{(1)}}{\partial t^2} = \mu_0 \frac{\partial^2 \tilde{\mathbf{P}}^{\mathrm{NL}}}{\partial t^2}. \tag{2.37}$$

Considering first the case of a lossless, dispersionless, and isotropic medium, we can express the relation between $\tilde{\mathbf{D}}^{(1)}$ and $\tilde{\mathbf{E}}$ as:

$$\tilde{\mathbf{D}}^{(1)} = \epsilon^{(1)} \epsilon_0 \tilde{\mathbf{E}}, \tag{2.38}$$

where $\epsilon^{(1)}$ is a real scalar constant. The wave equation is now given as:

$$\nabla^2 \tilde{\mathbf{E}} - \frac{\epsilon^{(1)}}{c^2} \frac{\partial^2 \tilde{\mathbf{E}}}{\partial t^2} = \mu_0 \frac{\partial^2 \tilde{\mathbf{P}}^{\mathrm{NL}}}{\partial t^2}. \tag{2.39}$$

This equation has the form of a driven (i.e., inhomogeneous) wave equation - the nonlinear response of the medium, namely $\tilde{\mathbf{P}}^{\mathrm{NL}}$, acts as a source term. In the absence of this term, Eq.(2.39) has a solution of the form of a free wave propagating with velocity c/n, where $n = \sqrt{\epsilon^{(1)}}$ is considered as the linear part of refractive index of the medium.

For the case of a dispersive medium, we must consider each frequency component of the wave separately. Therefore, we represent the electric field, the linear displacement, and the nonlinear polarization by their Fourier-transforms:

$$\tilde{\mathbf{E}}(t) = \frac{1}{2\pi} \int \tilde{\mathbf{E}}(\omega) e^{i\omega t} d\omega \tag{2.40}$$

$$\tilde{\mathbf{D}}^{(1)}(t) = \frac{1}{2\pi} \int \tilde{\mathbf{D}}^{(1)}(\omega) e^{i\omega t} d\omega \tag{2.41}$$

$$\tilde{\mathbf{P}}^{\mathrm{NL}}(t) = \frac{1}{2\pi} \int \tilde{\mathbf{P}}^{\mathrm{NL}}(\omega) e^{i\omega t} d\omega \tag{2.42}$$

As well-known from classical electrodynamics [30], the linear displacement of a medium and the electric field are related by:

$$\tilde{\mathbf{D}}^{(1)}(\omega) = \epsilon_0 \epsilon^{(1)}(\omega) \tilde{\mathbf{E}}(\omega) \tag{2.43}$$

Introducing the Eqs.(2.40) through (2.43) into the Eq.(2.37), we obtain the inhomogeneous Helmholtz wave equation in the frequency domain:

$$\nabla^2\tilde{\mathbf{E}}(\omega) + \frac{\omega^2}{c^2}\epsilon^{(1)}(\omega)\tilde{\mathbf{E}}(\omega) = -\mu_0\omega^2\tilde{\mathbf{P}}^{\mathrm{NL}}(\omega). \tag{2.44}$$

For more simplifications, we assume the field to be linearly polarized and propagating in the z-direction as a plane wave. The wave equation has now become[3]:

$$\left[\frac{\partial^2}{\partial z^2} + \frac{\omega^2}{c^2}\epsilon^{(1)}(\omega)\right]E(\omega) = -\mu_0\omega^2 P^{NL}(\omega) \tag{2.45}$$

This is the fundamental equation in solving the problem of ultrashort pulse propagating in a dispersive medium. We will next consider the case of a linear medium, where the phenomena such as absorption, dispersion, group velocity dispersion, and diffraction effects, etc. are concerned. Then the nonlinear medium will be discussed. Nowadays, with the developments of modern laser systems producing ultrashort and ultrahigh-intensity laser pulses, the nonlinear optical phenomena become more and more popular and diversified. Therefore, we will only concentrate on some of the effects, which will be referred to later in this work.

2.3.2 Linear Propagation

In the case of linear optics, the term $P^{NL}(\omega)$ vanishes and the wave equation (2.45) has a simple form

$$\left[\frac{\partial^2}{\partial z^2} + \frac{\omega^2}{c^2}\epsilon^{(1)}(\omega)\right]E(\omega) = 0. \tag{2.46}$$

The general solution of (2.46) is:

$$E(\omega, z) = E(\omega, 0)e^{-ik(\omega)z}, \tag{2.47}$$

where $k(\omega)$ is a frequency-dependent factor determined by the dispersion relation

$$k(\omega) = \frac{\omega}{c}\sqrt{\epsilon^{(1)}(\omega)} = n\omega/c \tag{2.48}$$

Applying the SVEA and expanding the propagating factor $k(\omega)$ about the carrier frequency ω_l, we have

$$k(\omega) = k_l + k_l'\Omega + \frac{k_l''}{2}\Omega^2 + \cdots = k_l + \triangle k(\omega), \tag{2.49}$$

[3]For convenience, we are working in the scalar field approximation.

where

$$k_l = \frac{n(\omega)\omega_l}{c} = \frac{2\pi}{\lambda_l} n(\lambda_l) \tag{2.50}$$

$$k_l^{'} = \left.\frac{\partial k}{\partial \omega}\right|_{\omega_l} = \frac{n(\omega_l)}{c} + \frac{\omega_l}{c}\left.\frac{\partial n}{\partial \omega}\right|_{\omega_l} = \frac{n(\lambda_l)}{c} - \frac{\lambda_l}{c}\left.\frac{\partial n}{\partial \lambda}\right|_{\lambda_l} \tag{2.51}$$

$$k_l^{''} = \left.\frac{\partial^2 k}{\partial \omega^2}\right|_{\omega_l} = \frac{2}{c}\left.\frac{\partial n}{\partial \omega}\right|_{\omega_l} + \frac{\omega_l}{c}\left.\frac{\partial^2 n}{\partial \omega^2}\right|_{\omega_l} = \frac{\lambda_l^3}{2\pi c^2}\left.\frac{\partial^2 n}{\partial \lambda^2}\right|_{\lambda_l}. \tag{2.52}$$

In order for the SVEA to be valid, we order that the pulse envelope must not change significantly while travelling through a distance comparable with the wavelength $\lambda_l = 2\pi/k_l$ or

$$\left|\frac{\triangle k}{k_l}\right| \ll 1. \tag{2.53}$$

The Eq.(2.47) is now rewritten as

$$E(\omega, z) = E(\omega, 0) e^{-ik_l z} e^{-i\triangle k(\omega) z}. \tag{2.54}$$

The time evolution of the electric field in the pulse is then derived by Fourier-transforming of (2.54)

$$\begin{aligned} \tilde{\mathrm{E}}(t, z) &= \frac{1}{2\pi}\int E(\omega, z) e^{i\omega t} d\omega \\ &= \left\{\frac{1}{2\pi}\int E(\omega, 0) e^{i\Omega(t - k_l^{'} z)} e^{-i(\frac{1}{2}k_l^{''}\Omega^2 + \cdots)z} d\omega\right\} e^{i\omega_l(t - \frac{k_l z}{\omega_l})} \qquad (2.55) \\ &= \tilde{A}(t, z) e^{i\omega_l(t - \frac{k_l z}{\omega_l})}, \qquad (2.56) \end{aligned}$$

where $\tilde{A}(t, z)$ is the field envelope varying slowly in space and time, defined by the term in the curled brackets in Eq.(2.55). In the third exponential term of (2.55), it can be seen that the phase of carrier frequency ω_l is delayed by an amount $k_l z/\omega_l$ after propagating over a distance z. Because the phase is not measurable, this effect has no observable consequence. The quantity

$$v_p = \frac{\omega_l}{k_l} = \frac{c}{n(\omega_l)} \tag{2.57}$$

is called the phase velocity, measuring the propagation speed of the central wavelength component of the pulse in the medium. The first exponential term in (2.55) shows that after propagation over a distance of z the pulse envelope is delayed by an amount z/v_g with $v_g = 1/k_l^{'}$ being the group velocity. From (2.51), we have the

relationship between the phase and group velocity:

$$\frac{1}{v_p} = \frac{1}{v_g} + \frac{\lambda_l}{c}\frac{\partial n}{\partial \lambda}\bigg|_{\lambda_l}. \tag{2.58}$$

In the case of normal dispersion ($\frac{\partial n}{\partial \lambda} < 0$), $v_g < v_p$. The factor k_l'' is called the **G**roup **V**elocity **D**ispersion (GVD) parameter and relates to the group velocity v_g through

$$\frac{\partial v_g}{\partial \lambda} = \frac{\omega^2 v_g^2}{2\pi c} k_l''. \tag{2.59}$$

To study the influences of the GVD parameter k_l'' on the field envelope, we return to the wave equation for linear case written in time domain. This equation can be derived from (2.37) and reads

$$\left[\frac{\partial^2}{\partial z^2} - \frac{1}{c^2}\frac{\partial^2}{\partial t^2}\right] \mathrm{D}^{(1)}(z,t) = 0. \tag{2.60}$$

For further considerations, we expand $\epsilon^{(1)}(\omega)$ as series about ω_l, leading to the following form for the linear displacement (2.43)

$$D^{(1)}(\omega, z) = \epsilon_0 \left[\epsilon_l^{(1)} + \sum_{m=1}^{\infty} \frac{1}{m!}\frac{d^m \epsilon^{(1)}}{d\omega^m}\bigg|_{\omega_l} \Omega^m\right] E(\omega, z). \tag{2.61}$$

For convenient reasons, we transfer to a coordinate system (η, ξ) moving with the group velocity v_g:

$$\xi = z, \qquad \eta = t - \frac{z}{v_g}. \tag{2.62}$$

In the case of practical interest, where the dielectric constant changes slowly over the frequencies within the spectrum, terms with $m \geq 3$ in (2.49) and (2.61) can be neglected. By introducing (2.56) and the appropriate expression of (2.61) in the time domain into (2.60), we get the simple form of the wave equation [35] for the complex field envelope $\tilde{A}(\eta, \xi)$:

$$\left[\frac{\partial}{\partial \xi} - \frac{i k_l''}{2}\frac{\partial^2}{\partial \eta^2}\right] \tilde{A}(\eta, \xi) = 0, \tag{2.63}$$

For the case of zero GVD ($k_l'' = 0$), the pulse envelope does not change its shape in the local system. That means, in the laboratory system the pulse propagates at the group velocity without any distortion.

For $k_l'' \neq 0$, we can solve the Eq.(2.63) in the frequency domain by Fourier-transforming

the field envelope $\tilde{A}(\eta, \xi)$ as

$$\tilde{A}(\eta, \xi) = \frac{1}{2\pi} \int A(\omega, \xi) e^{-i\omega\eta} d\omega \tag{2.64}$$

Inserting (2.64) in (2.63) we have the wave equation for field envelope in frequency domain

$$\left[\frac{\partial}{\partial \xi} + \frac{i k_l'' \omega^2}{2} \right] A(\omega, \xi) = 0, \tag{2.65}$$

and its solution is simply given as

$$A(\omega, \xi) = A(\omega, o) e^{-\frac{i}{2} k_l'' \omega^2 z}. \tag{2.66}$$

As seen from (2.66), GVD leads the pulse to develop a spectral phase with a quadratic frequency dependence, resulting in linear chirp. k_l'' is thus also called the *linear chirp parameter*. From the example of Gaussian pulse given previously, we know that this is responsible for the broadening of the pulse envelope.

2.3.3 Nonlinear Optics

In this section we will discuss some of nonlinear phenomena occurring with the presence of ultrashort laser pulses. Soon after the first laser was detected by Maiman [1] in 1960, the **S**econd **H**armonic **G**eneration (SHG) was first observed experimentally with the work of Franken and coworkers [36]. It occurs as a result of the part of the atomic response that depends quadratically on the electric field. Consequently, the intensity generated at the second harmonic frequency tends to increase as the square of the intensity of the applied field. We now proceed to study in detail the **S**um **F**requency **G**eneration (SFG) as the general case of the SHG. We will show relationship between intensity of the SFG-wave and the incident waves, which is very important for the theories of the correlation technique described later in this work. At the end of the section, some typical third-order effects useful for evaluating the experiment results will be also discussed.

2.3.3.1 The Sum Frequency Generation

Considering the case of SFG in a isotropic lossless medium with quadratic optical nonlinearity. The applied waves are assumed to fall onto the nonlinear medium at normal incidence. We suppose that the solution for (2.39) has the form similar to (2.56)

$$\mathrm{E}_3(z, t) = A_3(z, t) e^{i(\omega_3 t - k_3 z)} + \mathrm{c.c}, \tag{2.67}$$

where

$$k_3 = k_3(\omega_3) = \frac{n_3\omega_3}{c}, \qquad n_3 = \sqrt{\epsilon^{(1)}(\omega_3)}, \tag{2.68}$$

Here $A_3(z,t)$ is assumed to satisfy the inequality of SVEA in space

$$\left|\frac{\partial^2 A_3}{\partial z^2}\right| \ll \left|k_3\frac{\partial A_3}{\partial z}\right|, \tag{2.69}$$

and time domain

$$\left|\frac{\partial^2 A_3}{\partial t^2}\right| \ll \left|\omega_3\frac{\partial A_3}{\partial t}\right|. \tag{2.70}$$

Similarly, we represent the polarization and the incident waves as

$$\mathrm{P}_3^{\mathrm{NL}}(z,t) = P_3^{NL}(z,t)e^{i(\omega_3 t - k_3 z)} + \mathrm{c.c} \tag{2.71}$$

$$\mathrm{E}_j(z,t) = A_j(z,t)e^{i(\omega_j t - k_j z)} + \mathrm{c.c} \qquad (j=1,2) \tag{2.72}$$

and the amplitude of the nonlinear polarization [37]

$$P_3^{NL} \equiv P_3^{(2)} = 4\epsilon_0 d_{\mathrm{eff}} A_1 A_2 e^{-i(k_1+k_2)z}, \tag{2.73}$$

where d_{eff} is the so-called effective d-coefficient dependent on structure of the nonlinear medium and is tabulated elsewhere [37].
Introducing the Eqs.(2.67) through (2.73) into (2.39), we obtain the so-called *coupled-amplitude equation* in the first-order approximation of dispersion theory

$$\frac{\partial A_3}{\partial z} + \frac{1}{u_3}\frac{\partial A_3}{\partial t} = \frac{2\omega_3 d_{\mathrm{eff}}}{in_3 c}A_1 A_2 e^{-i\delta k z}, \tag{2.74}$$

where u_3 is the group velocity of the sum-frequency wave ω_3 and $\delta k = k_1 + k_2 - k_3$ is called the *wave vector mismatch*. When the variation of the ω_1 and ω_2 waves must also be taken into consideration, we can derive the analogous equations for each of these frequencies:

$$\frac{\partial A_1}{\partial z} + \frac{1}{u_1}\frac{\partial A_1}{\partial t} = \frac{2\omega_1 d_{\mathrm{eff}}}{in_1 c}A_3 A_2^* e^{i\delta k z}, \tag{2.75}$$

and

$$\frac{\partial A_2}{\partial z} + \frac{1}{u_2}\frac{\partial A_2}{\partial t} = \frac{2\omega_2 d_{\mathrm{eff}}}{in_2 c}A_3 A_1^* e^{i\delta k z}, \tag{2.76}$$

with u_1 and u_2 being the group velocity of the ω_1- and ω_2-waves, respectively.
In the case of monochromatic planar incident waves[4], the time-derivative terms $\partial A_j/\partial t$ (with $j = 1,2,3$) in the coupled-amplitude equations vanish and the resulting equations can be solved exactly using the Jacobi elliptic function [38]. By assuming the applied waves to be undepleted by the nonlinear interaction, Boyd [31] shows

[4] Also called the *Infinite Plane Wave Approximation*.

that the intensity of the sum-frequency wave is proportional to product of these of the applied waves

$$I_3 \sim I_1 I_2 L^2 \mathrm{sinc}^2(\delta k L/2), \tag{2.77}$$

where I_j are the intensity of the ω_j-wave, respectively, and L is the distance of the nonlinear medium, over which the waves interact with each other. The intensity I_3 reaches its maximum value I_{3max} when $\delta k = 0$ or also called the *perfect phase-matching* (PM) condition. A more detailed discussion of phase-matching will be described later in the section of conversion efficiency consideration.
In the case of ultrashort laser pulses, a generally exact solution for these equations is impossible. These short pulses have an appropriate spectral width and it is not possible to satisfy the phase-matching condition for all of the possible frequency components in the spectrum. Here the group velocity mismatch comes into play and complicates the conversion processes. For simplicity, we will next discuss the case of identical incident waves or the second harmonic generation, whose processes, in many respects, are similar to the sum-frequency process. More discussions about SFG of ultrashort pulses can be found in [31, 39] and the references therein.

2.3.3.2 The Second Harmonic Generation

We now proceed to derive the coupled-amplitude equations for the second-harmonic (SH) processes. The fundamental and SH waves can also be described as

$$\begin{aligned} \mathrm{E}_1(z,t) &= A_1(z,t)e^{i(\omega t - k_1 z)} + \mathrm{c.c} && (2.78)\\ \mathrm{E}_2(z,t) &= A_2(z,t)e^{i(2\omega t - k_2 z)} + \mathrm{c.c} && (2.79) \end{aligned}$$

The electric field in the medium is then written in the form

$$\begin{aligned} \mathrm{E}(z,t) &= \mathrm{E}_1(z,t) + \mathrm{E}_2(z,t) \\ &= A_1(z,t)e^{i(\omega t - k_1 z)} + A_2(z,t)e^{i(2\omega t - k_2 z)} + \mathrm{c.c} && (2.80) \end{aligned}$$

The nonlinear polarization can be represented as

$$\begin{aligned} \mathrm{P}^{\mathrm{NL}}(z,t) &= \mathrm{P}_1^{\mathrm{NL}}(z,t) + \mathrm{P}_2^{\mathrm{NL}}(z,t) \\ &= P_1^{NL}(z,t)e^{i(\omega t - k_1 z)} + P_2^{NL}(z,t)e^{i(2\omega t - k_2 z)} + \mathrm{c.c}, && (2.81) \end{aligned}$$

where the expressions for P_j^{NL} (with $j = 1, 2$) are given by [37]

$$\begin{aligned} P_1^{NL} &= 4\epsilon_0 d_{\mathrm{eff}} A_2 A_1^* e^{i(k_1 - k_2)z} && (2.82)\\ P_2^{NL} &= 2\epsilon_0 d_{\mathrm{eff}} A_1^2 e^{-2ik_1 z}. && (2.83) \end{aligned}$$

Substituting the equations (2.80) and (2.81) into (2.39), we obtain the coupled-amplitude equations for SHG

$$\frac{\partial A_1}{\partial z}+\frac{1}{u_1}\frac{\partial A_1}{\partial t} = -i\gamma_1 A_2 A_1^* e^{i\delta k z} \tag{2.84}$$

$$\frac{\partial A_2}{\partial z}+\frac{1}{u_2}\frac{\partial A_2}{\partial t} = -i\gamma_2 A_1^2 e^{-i\delta k z}, \tag{2.85}$$

where

$$\delta k = 2k_1 - k_2 \tag{2.86}$$

is the phase mismatch and

$$\gamma_j = \frac{2\omega d_{\text{eff}}}{n_j c} \qquad \text{with} \quad j = 1, 2. \tag{2.87}$$

Group velocity matching. We first consider the simplest case, where the phase-matching and group velocity matching conditions are simultaneously satisfied:

$$\delta k = 0 \qquad \text{and} \qquad u = u_1 = u_2. \tag{2.88}$$

We transfer to the local system (2.62) and introduce the real amplitudes and phases $A_j(\eta,\xi) = a_j(\eta,\xi)e^{i\varphi_j}$. The solutions for set of Eqs.(2.84) and (2.85) are [39]

$$a_1(\eta,\xi) = a_{10}(\eta)\text{sech}[\gamma a_{10}(\eta)\xi], \tag{2.89}$$

$$a_2(\eta,\xi) = a_{10}(\eta)\tanh[\gamma a_{10}(\eta)\xi], \tag{2.90}$$

$$\varphi_1(\eta,\xi) = \varphi_{10}(\eta), \tag{2.91}$$

$$\varphi_2(\eta,\xi) = 2\varphi_1(\eta) - \pi/2, \tag{2.92}$$

where $a_{10}(\eta) = a_1(\eta,0)$ and $\gamma = \gamma_1 = \gamma_2$.
In the undepleted-pump approximation (UPA), the fundamental wave is assumed constant along the whole interaction length. The SH wave then becomes

$$a_2(\eta,\xi) = \gamma z a_{10}^2(\eta). \tag{2.93}$$

Using (2.19), we have the appropriate intensity relation between the interacting waves:

$$I_2(t,z) = \frac{\gamma^2 z^2}{2\epsilon_0 c n_1} I_1^2(t-\frac{z}{u}) \tag{2.94}$$

The intensity of SH wave is quadratically proportional to the intensity of the fundamental wave and to the interaction length. This results in shortening the SH pulse duration. For a fundamental Gaussian-shaped pulse $a_{10}(\eta) = a_0 e^{-t^2/\tau_G^2}$ with pulse

duration $\tau_1 = \sqrt{2\ln 2}\tau_G$, the SH pulse duration is $\tau_2 = \tau_1/\sqrt{2}$.

Group velocity mismatch. In fact, the group velocity matching conditions are not satisfied ($u_1 \neq u_2$). Applying the UPA for Eqs. (2.84) and (2.85), we obtain the solutions [39]

$$A_2(t,z) = -i\gamma_2 \int_0^z A_{10}^2(t - z/u_2 + \triangle u^{-1}\xi)e^{i\delta k\xi}d\xi, \tag{2.95}$$

where

$$\triangle u^{-1} = \frac{1}{u_2} - \frac{1}{u_1} \tag{2.96}$$

is called the group mismatch and

$$A_{10}(t) = A_1(t,0). \tag{2.97}$$

For more simplicity, we assume the fundamental amplitude is a Gaussian linear-chirp pulse

$$A_{10}(t) = a_0 e^{-(1+i\alpha)t^2/\tau_G^2}. \tag{2.98}$$

The SH intensity can be obtained from (2.95) for the case of perfect phase-matching $\delta k = 0$:

$$I_2(t,z) = \frac{\gamma_2^2 z^2}{2\epsilon_0 c n_1} I_1^2(t - \frac{z}{u_2})\mathrm{sinc}^2\left[\frac{\alpha z \triangle u^{-1}}{\tau_G^2}(t - \frac{z}{u_2})\right]. \tag{2.99}$$

It can be seen from the above equation that for the case of unchirped Gaussian pulses, $\alpha = 0$, the SH intensity does not depend on the group mismatch $\triangle u^{-1}$. For strongly chirped pulses, because of the group velocity mismatch effect, the nonlinear medium acts as the frequency-filter, whose bandwidth is reversely proportional to group mismatch. Generally, the filter function depends both on the fundamental and SH frequencies.

2.3.3.3 Conversion Efficiency Consideration

Phase-matching. In relationship with the other aspects which are important for achieving high conversion efficiency, the phase-matching condition briefly discussed in SFG-process will be considered here in more detail. In this work, the conversion efficiency of the SFG is defined from Eq.(2.77) as:

$$\Pi = \frac{I_3}{I_{3max}} = \mathrm{sinc}^2(\delta k L/2) \tag{2.100}$$

where

$$\delta k = k_1 + k_2 - k_3 = \frac{1}{c}[n_1\omega_1 + n_2\omega_2 - n_3\omega_3]. \tag{2.101}$$

If $\delta k = 0$, i.e

$$n_1\omega_1 + n_2\omega_2 - n_3\omega_3 = 0, \tag{2.102}$$

the SFG-process is said to be perfect phase-matching and the conversion efficiency reaches its maximal value 1. When phase-mismatch occurs, $\delta k \neq 0$, the conversion efficiency decreases severely and can be seen in figure 2.2. By replacing $\omega_3 = \omega_1 + \omega_2$,

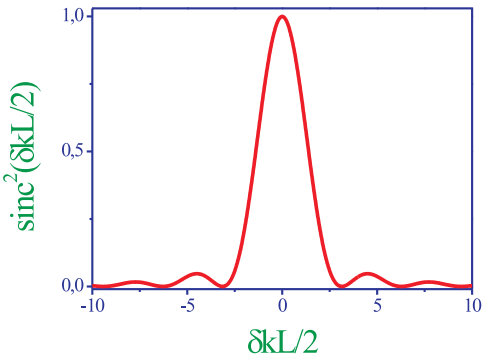

Fig. 2.2: The effect of phase-mismatch on conversion efficiency of the SFG.

we obtain:

$$n_3 - n_2 = (n_1 - n_2)\frac{\omega_1}{\omega_3} \tag{2.103}$$

As shown by Boyd [31], in the normally dispersive materials the phase-matching condition is impossible because of the increase of the refractive index with frequency. One of the most commonly used techniques for achieving the phase-matching is *angle tuning*, which exploits the birefringent property of nonlinear crystals. Birefringence is the dependence of the refractive index on the direction of polarization of the input wave. By tuning the angular orientation of the crystal with respect to the propagation direction of input waves, one can find the polarized direction of the highest-frequency ω_3 which provides the lower of the two possible refractive indices. There are two types of angle phase-matching [40] illustrated in figure 2.3:

- Type I phase-matching: the two input waves have the same polarization
- Type II phase-matching: the polarizations of the two input waves are orthogonal

For instance, **B**eta **B**arium **B**orate (BBO) crystal is a negative uniaxial crystal ($n_e < n_o$). Therefore, the polarization direction of the ω_3 wave in the BBO crystal is in the extraordinary direction and the phase-matching equations for type I and

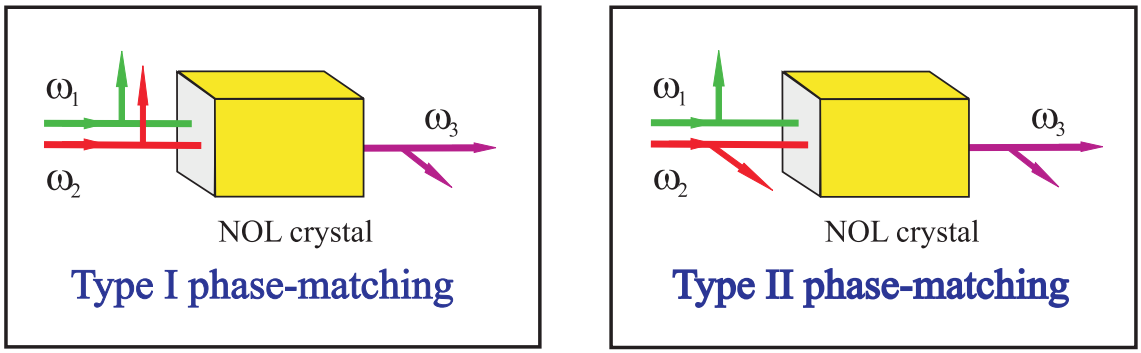

Fig. 2.3: Type I and II of phase-matching of the SFG-process. The ω_1 and ω_2- waves are the input waves, and ω_3-wave is the generated sum-frequency wave ($\omega_3 = \omega_1 + \omega_2$). The arrows show the polarization vectors of respective waves (NOL crystal: nonlinear crystal).

II, respectively, are [31]:

$$n_3^e\omega_3 = n_1^o\omega_1 + n_2^o\omega_2 \quad \text{(Type I: } ooe\text{)} \tag{2.104}$$

$$n_3^e\omega_3 = n_1^e\omega_1 + n_2^o\omega_2 \quad \text{(Type II: } eoe\text{)}, \tag{2.105}$$

where the indices o and e imply the ordinary and extraordinary directions in the crystal, respectively. By each nonlinear crystal with certain polarization of input waves, there is an optimum phase-matching angle θ_m made of the propagation direction and the optical axis of the nonlinear crystal. For the purpose of later use, some useful angle phase-matching formulas for BBO crystal are given in table 2.1 [37].

NL process	Phase-matching angle
SHG(ooe)	$\sin^2\theta_m = \dfrac{(n_{2\omega}^e)^2}{(n_\omega^o)^2}\left[\dfrac{(n_{2\omega}^o)^2-(n_\omega^o)^2}{(n_{2\omega}^o)^2-(n_{2\omega}^e)^2}\right]$
SFG(eoe)	$\dfrac{n_3^o}{\sqrt{1+\left[\dfrac{(n_3^o)^2}{(n_3^e)^2}-1\right]\sin^2\theta_m}} - \dfrac{(\lambda_3/\lambda_1)n_1^o}{\sqrt{1+\left[\dfrac{(n_1^o)^2}{(n_1^e)^2}-1\right]\sin^2\theta_m}} = (\lambda_3/\lambda_2)n_2^o$

Table 2.1: The phase-matching angles of BBO crystal for the SHG (Type I) and SFG (Type II) processes

Crystal acceptance angle. If the input wave propagates with an angle θ deviating from the phase-matching angle θ_m, δk is different from zero causing inefficient harmonic generation. The angular sensitivity is determined by an acceptance angle

$\triangle\theta$ defined by the condition[5]

$$|\delta k L| = 2\pi, \tag{2.106}$$

at which the sinc^2-function in Eq.(2.100) gets its first zero. For the case of SHG in a negative uniaxial crystal, the acceptance angle is given as [41]:

$$\triangle\theta = \frac{2(\lambda_\omega/L)}{(n^o_\omega)^2[(n^e_{2\omega})^{-2} - (n^o_{2\omega})^{-2}]\sin 2\theta_m} \tag{2.107}$$

Walk-off. Due to the birefringence of nonlinear crystals, the extraordinary wave n^e experiences Pointing vector walk-off (Fig. 2.4) and as the result, if the input laser beam size is small, the generated harmonic beam and the fundamental beam will be separated at a walk-off angle ρ in the crystal, causing low conversion efficiency. Therefore, the walk-off effect must be taken into account when one tries to decrease the beam size (for instance, by focusing the laser beam) to enhance the efficient conversion due to increase in intensity.

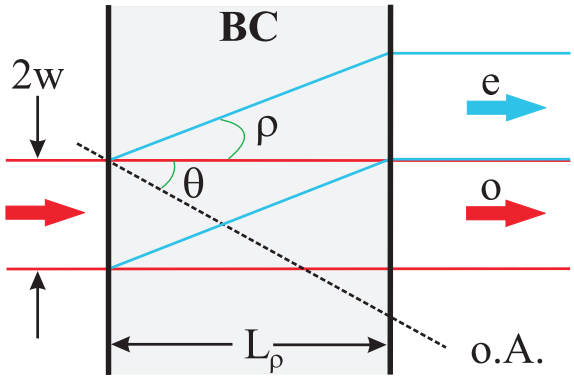

Fig. 2.4: The walk-off effect due to double refraction in birefringent crystals (BC: birefringent crystal; o.A.: optical axis; w: the beam radius; $\theta = (\vec{k}$,o.A.)).

The walk-off angle for negative uniaxial crystal is given as [41]:

$$\tan\rho = \frac{[(n^o)^2 - (n^e)^2]\tan\theta}{(n^e)^2 + (n^o)^2\tan^2\theta}. \tag{2.108}$$

The e- and o-beams become physically separated in a so-called *walk-off length* L_ρ given as:

$$L_\rho = \frac{2\mathrm{w}}{\tan\rho}. \tag{2.109}$$

For BBO crystal with $n^o = 1.69298$, $n^e = 1.66051$, $\theta_m = 29.2^0$ (phase matching angle-type I) at 400 nm central wavelength and 1 mm beam diameter, we have:

$$\rho = 16.7 \text{ mrad} \quad \text{and} \quad L_\rho = 6 \text{ cm}. \tag{2.110}$$

[5] In some literatures, the acceptance angle is determined by the equation: $|\delta k L| = \pi$.

Group mismatch. Generally, the interacting pulses travel with different group velocities in nonlinear medium resulting in pulse broadening effect (Fig. 2.5). Over a certain distance, they may no longer physically overlap and hence the conversion efficiency will be dramatically reduced.

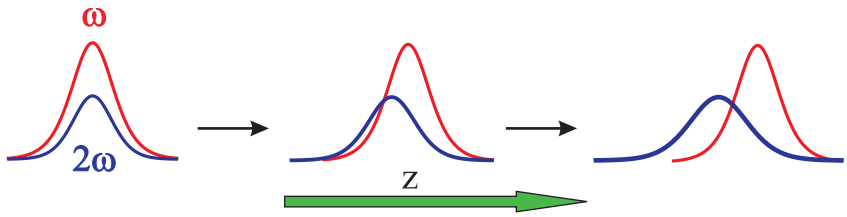

Fig. 2.5: The pulse broadening effect due to group velocity mismatch of SGH process

To keep efficient conversion without significant pulse broadening, it is recommended to use nonlinear crystals, whose thickness is less than the pulse width divides group mismatch, i.e:

$$L_c \leq \frac{\tau_p}{\triangle u^{-1}}. \tag{2.111}$$

For example for BBO:

$$\begin{aligned} 800\text{ nm:} \quad \frac{1}{u_1} &= 56.09 \quad \text{ps/cm} \\ 400\text{ nm:} \quad \frac{1}{u_2} &= 58.01 \quad \text{ps/cm} \\ \triangle u^{-1} &= 1.92 \quad \text{ps/cm} \\ \tau_p &= 60 \quad \text{fs} \\ \Rightarrow \quad L_c &\leq 300 \quad \mu\text{m} \end{aligned} \tag{2.112}$$

2.3.3.4 The Third-Order Effects

The third-order effects, which can be found in both centrosymmetric and noncentrosymmetric materials, are related to the third-order susceptibility term of the expansion of the polarization vector (Eq.2.7). When an intense ultrashort laser pulse passes into an isotropic medium, its nonlinear refractive index can be generally written as

$$n = n_0 + n_2 I(\vec{r}, t), \tag{2.113}$$

where n_0 is the linear refractive index of the materials, n_2 is the nonlinear index coefficient and is usually given in [cm^2/W]. We will separately consider the effects caused by the spatial and temporal dependence of the laser intensity. The general treatments for ultrashort laser pulses are very complicated and beyond the scope of this work. More approximate discussions can be found in, for example, [31, 39].

Here, for the reasons of simplicity, we will investigate the propagation of a Gaussian laser beam in a third-order nonlinear material. The results, however, still hold for the case of ultrashort laser pulses.

Kerr Lens Effects. The refractive index distribution in this case is

$$n(r) = n_0 + n_2 I(r), \qquad \text{with} \quad I(r) = e^{-2r^2/w^2}. \tag{2.114}$$

As seen from (2.114), for a positive n_2 the refractive index has a maximum value at the center by $r = 0$ and decreases with increasing r. After propagating over a distance e the beam has a optical path $Ł(r) = n(r)e$. The constant e is replaced by a variable one such that its product with a constant refractive index remains the same optical path:

$$Ł(r) = n(r)e = e(r)n \tag{2.115}$$

or

$$e(r) = \frac{en(r)}{n}. \tag{2.116}$$

That means, the medium reacts as a Gaussian lens, which focuses the laser beam. This focusing process becomes stronger along the path because the focused beam increases the focal power of the dynamical lens. The increase of the focusing stops when the diameter is so small that the linear diffraction is large enough to balance the Kerr effect. This effect, also called *self-focusing*, is very important in the understanding of self-mode-locking, which occurs in Ti:Al_2O_3 lasers. If the path through the medium is sufficiently long, the beam will be focused to a small filament (beam collapse), and the medium will be usually damaged via avalanche ionization. The critical power level for Gaussian beam at which beam collapse will happen is given by [42]

$$P_{\text{cr}} = \frac{\kappa\lambda^2}{8\pi n_0 n_2}, \tag{2.117}$$

where κ is a correction factor accounting for the fact the severity of nonlinear phase distortion[6].

Self Phase Modulation. If the time-dependent laser intensity must be taken into account, we can write the refractive index in the form

$$n(t) = n_0 + n_2 I(t), \qquad \text{with} \quad I(t) = e^{-2t^2/\tau_G^2}. \tag{2.118}$$

To study the influence of this time-varying index on the frequency of laser beam, we consider now the simple case of a plane wave propagating in the z direction of a

[6]The initial Gaussian profile is deformed during the self-focusing process.

nonlinear medium:

$$\mathrm{E}(t,z) = A_0 e^{i(\omega_l t - kz)}, \qquad k = \frac{\omega_l n(t)}{c}. \tag{2.119}$$

The instantaneous frequency is

$$\omega(t) = \frac{\partial}{\partial t}(\omega_l t - kz) = \omega_l \left[1 - \frac{n_2 z}{c}\frac{\partial I(t)}{\partial t}\right] \tag{2.120}$$

and the frequency variation

$$\delta\omega(t) = \omega(t) - \omega_l = -\frac{n_2 \omega_l z}{c}\frac{\partial I(t)}{\partial t}. \tag{2.121}$$

With $n_2 > 0$, new low frequencies are created in the leading edge of the pulse envelope and new high frequencies are created in the trailing edge (Fig. 2.6). These

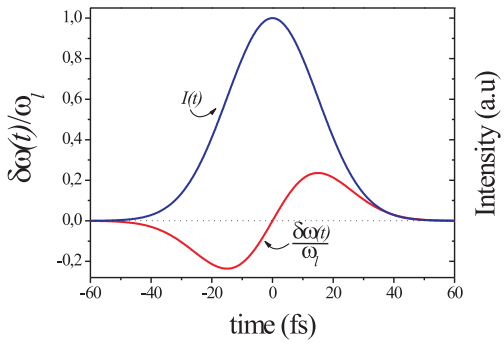

Fig. 2.6: The instantaneous frequency as function of time for the case of $n_2 > 0$.

new frequencies are created inside the original pulse envelope, result a chirped pulse and, therefore, open the way to spectral broadening. Using the SPM for optical compression technique man has generated ultrashort laser pulses less than 10 fs in duration.

2.4 Correlation Techniques

2.4.1 The Intensity Correlations

We can easily determine the temporal profile $I_s(t)$ of an optical signal by correlating it with a shorter (reference) pulse of known shape $I_r(t)$. The intensity cross-correlation reads:

$$A_c(\tau) = \int I_s(t-\tau) I_r(t) dt. \tag{2.122}$$

The Fourier-transform of the intensity profiles is defined as[7]:

$$\tilde{I}_j(\Omega) = \int I_j(t) e^{-i\Omega t} dt, \qquad (j = r, s). \tag{2.123}$$

The Fourier transform of the correlation Eq.(2.122) can be now written as

$$\tilde{A}_c(\Omega) = \tilde{I}_r(\Omega)\tilde{I}_s^*(\Omega), \tag{2.124}$$

and consequently the temporal profile $I_s(t)$ can be formally determined by

$$\begin{aligned} I_s(t) &= \frac{1}{2\pi}\int \tilde{I}_s(\Omega) e^{i\Omega t} d\Omega \\ &= \frac{1}{2\pi}\int \left[\frac{\tilde{A}_c(\Omega)}{\tilde{I}_r(\Omega)}\right]^* e^{i\Omega t} d\Omega. \end{aligned} \tag{2.125}$$

To increase the signal-to-noise ratio, the reference pulse should be the (temporally) shortest pulse of the two correlated pulses. In ideal case of the Dirac-function $\delta(t)$, the correlation becomes

$$A_c(\tau) = \int I_s(t)\delta(t-\tau)dt = I_s(\tau). \tag{2.126}$$

So the shape of the correlation is identical to that of the signal $I_s(t)$. One general disadvantage of correlation techniques is that the pulse shape has to be assumed and thus the accuracy of the measurements depends strongly upon how well one chooses the pulse shape. The most widely used pulse shapes are sech^2- and Gaussian shapes.

2.4.1.1 The Intensity Autocorrelation

To measure a pulse duration one needs a shorter reference pulse. But how one can measure the shortest pulse? Therefore, it is necessary to consider the limit where the signal itself has to be used as reference pulse. In such the case with $I(t) = I_s(t) = I_r(t)$, we have the so-called intensity autocorrelation[8]

$$A_{ac}(\tau) = \int I(t)I(t-\tau)dt, \tag{2.127}$$

and its Fourier-transform

$$\tilde{A}_{ac}(\Omega) = |\tilde{I}(\Omega)|^2. \tag{2.128}$$

[7]Here $\tilde{I}_j(\Omega)$ should not be confused with the spectral intensity $S(\Omega)$ given by (2.20). Spectral intensity is measurable, the FT of intensity profile, however, is not!

[8]In this case, we have the intensity autocorrelator without background or noncolinear intensity autocorrelator. The intensity autocorrelator with background will be also referred to later in the section of interferometric autocorrelator.

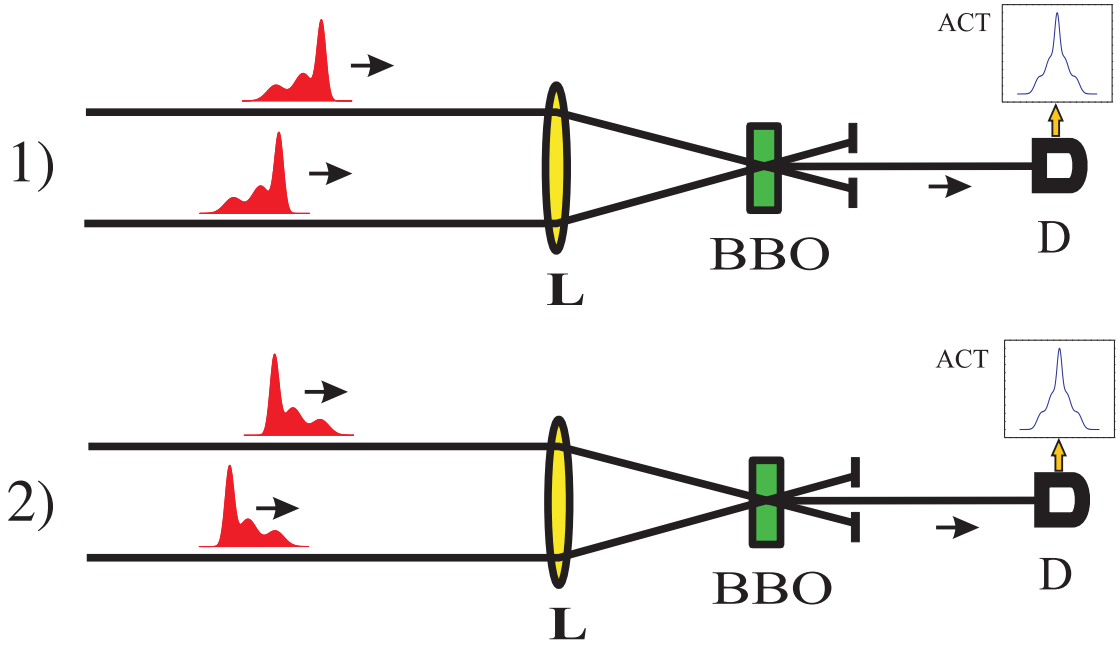

Fig. 2.7: The schematic experiment setups of a intensity autocorrelator showing the ambiguity of time direction of the pulses. The laser pulses with shape of different asymmetries can have similar intensity autocorrelations (L: Lens, BBO: Beta-Barium Borate crystal; D: detector; ACT: autocorrelation trace).

As directly seen from (2.128), the Fourier transform of the autocorrelation is a real function, implying a symmetric function, $A_{ac}(\tau) = A_{ac}(-\tau)$, in the time domain. Invented in the 1960s, autocorrelation was the first technique used to measure the intensity versus time of an ultrashort pulse. However, it provides no information on the phase of the pulses and shows an ambiguity of time direction (Fig. 2.7).

Despite the basic disadvantages referred to above the intensity autocorrelation, because of its easy implementation, is the most widely used diagnostic technique. The autocorrelation techniques are generally related to second-order nonlinear effects of media, such as SHG, two-photon absorption, two-photon ionization, etc. phenomena. Basically, the technique involves splitting a laser beam into two replicas, variably delaying one with respect to the other and overlapping them in a nonlinear medium to produce SH radiation. The signal is then recorded by an integrating detector. As discussed previously, the intensity of SH signal is proportional to the product of the intensities $I(t)$ of the two beams (only in the case of UPA). In other words, the nonlinear medium and the detector act as an "operator", which correlates the two beams with each other as a function of delay τ. The normalized intensity autocorrelation is then given by:

$$A_{ac}(\tau) = \frac{\int I(t)I(t-\tau)dt}{\int I^2(t)dt} \tag{2.129}$$

For a Gaussian-shaped pulse with the intensity given as

$$I(t) = e^{-2t^2/\tau_G^2}, \tag{2.130}$$

and the pulse duration

$$\tau_p = \sqrt{2\ln 2}\tau_G, \tag{2.131}$$

the Eq.(2.129) becomes

$$A_{ac}^G(\tau) = e^{-\tau^2/\tau_G^2}, \tag{2.132}$$

and its FWHM

$$\tau_A = \sqrt{\ln 2}\tau_G = \frac{\tau_p}{\sqrt{2}}. \tag{2.133}$$

In general, the pulse duration can be obtained from the known ratio between the FWHM of the pulse and that of the autocorrelation. This ratio depends on the assumed pulse shape and is equal to $\sqrt{2}$ for Gaussian-shaped pulse (2.133).

2.4.1.2 The Higher-Order Intensity Correlations

Generally relying on the higher-order nonlinear effects such as higher harmonic generation, multiphoton absorption, multiphoton ionization and optical Kerr effect, the normalized higher-order intensity correlation (HOIC) of order $(n+1)$ can be defined as [35]

$$A_{n+1}(\tau) = \frac{\int I(t+\tau)I^n(t)dt}{\int I^{n+1}(t)dt}. \tag{2.134}$$

For $n > 1$, the correlation function (2.134) has the same symmetry as the pulse. In addition, it was shown that third-order intensity correlations are sufficient to determine the time-dependent intensity of a laser pulse and all HOICs can be described in terms of the third one [43]. Nevertheless, HOICs have become widely used and powerful tools in ultrashort pulse measurements, specially for the cases of lasers with very high intensity. The reason is that for most pulse shapes with a well-defined maximum, $\lim_{n\to\infty} I^n(t) \propto \delta(t)$ and the correlation $A_n(\tau)$ produces a good approximation to the pulse shape $I(t)$ [see (2.126)]. As shown in Fig. 2.8, only with $n = 19$ the correlation trace has already merged with the original laser pulse.

As a specific case of high-order correlation techniques, the third-order correlation will be discussed in more details in the next chapter.

2.4.2 The Interferometric Correlations

To produce the shortest pulses in a laser system, one has to compensate linear, quadratic, or even higher-order chirp introduced by intracavity materials [35]. As a

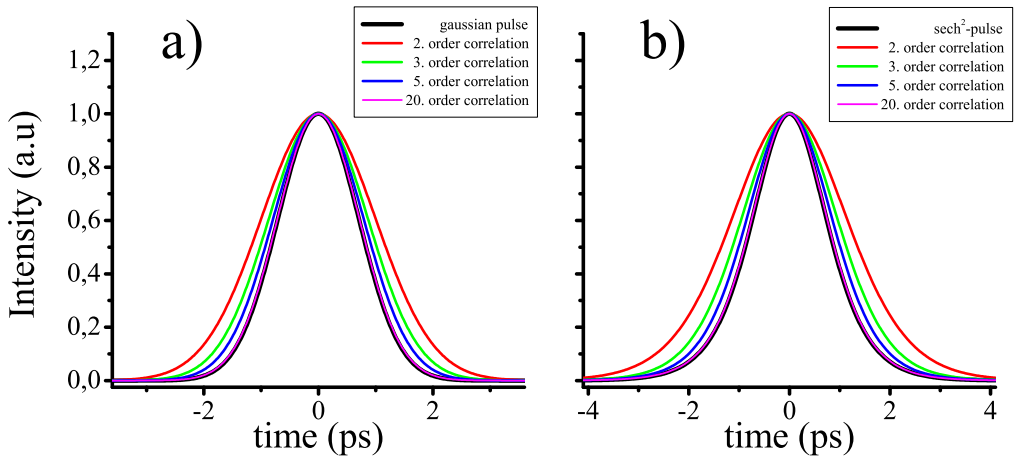

Fig. 2.8: The normalized correlations of various orders for gaussian and sech^2-pulse shapes.

result, techniques, which are able to reveal the phase structure of a laser pulse, must be required. A simple method is to use second-order interferometric correlators. In principle, such a correlator is similar to a Michelson or Mach-Zehnder interferometer [44] except for the intensity detector being substituted by a nonlinear detector (a combination of a nonlinear medium and an intensity detector)(Fig. 2.9).
For simplicity, the interferometric autocorrelator using SHG will be next discussed in detail[9]. The interferometric autocorrelation $A_2(\tau)$ is defined by

$$A_2(\tau) = \int |[\mathrm{E}(t) + \mathrm{E}(t-\tau)]^2|^2 dt. \tag{2.135}$$

Substituting the expression (2.16) for the electric field, one obtains the following decomposition

$$A_2(\tau) = K_0(\tau) + \Re e\Big\{4K_1(\tau)e^{i\omega_l\tau}\Big\} + \Re e\Big\{2K_2(\tau)e^{2i\omega_l\tau}\Big\}, \tag{2.136}$$

[9]The theory and experiments of THG interferometric autocorrelation with some advantages have been recently reported in the work of Meshulach *et. al.* [45].

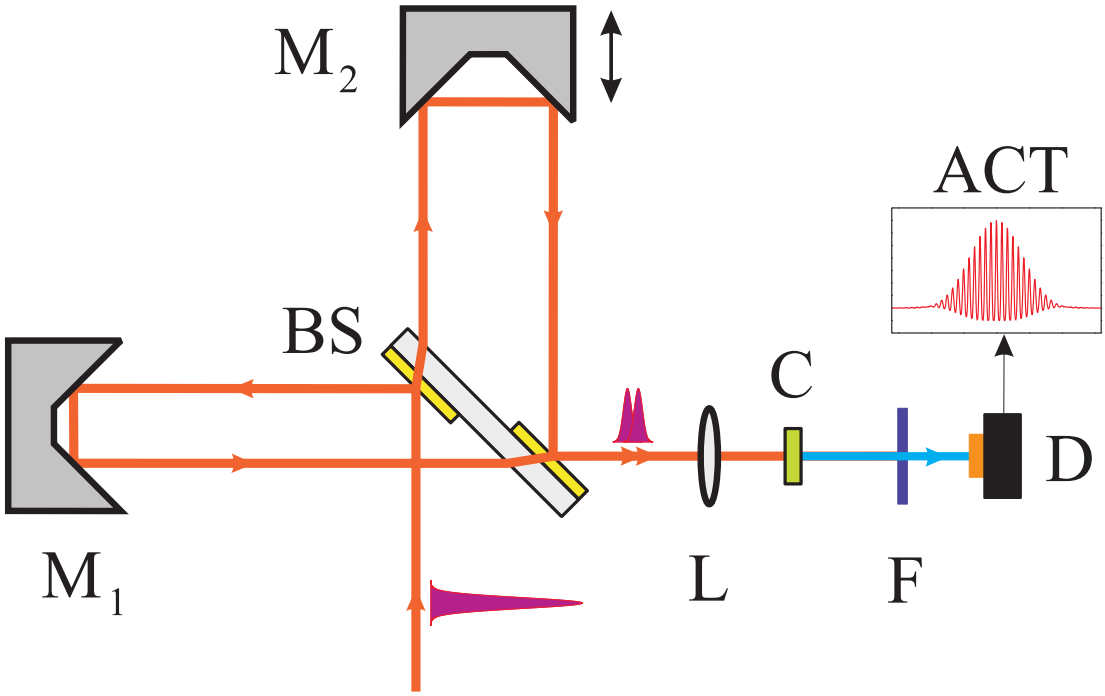

Fig. 2.9: Setup of a interferometric autocorrelator (M_1, M_2: HR mirrors; BS: Beam splitter; L: Lens; C: nonlinear crystal; F: fundamental-blocking filter; D: detector; ACT: the interferometric autocorrelation trace).

where

$$K_0(\tau) = \int dt \left\{ A^4(t-\tau) + A^4(t) + 4A^2(t-\tau)A^2(t) \right\} \tag{2.137}$$

$$K_1(\tau) = \int dt \left\{ A(t-\tau)A(t) \left[A^2(t-\tau) + A^2(t) e^{i[\varphi(t-\tau)-\varphi(t)]} \right] \right\} \tag{2.138}$$

$$K_2(\tau) = \int dt \left\{ A^2(t-\tau)A^2(t) e^{2i[\varphi(t-\tau)-\varphi(t)]} \right\} \tag{2.139}$$

At zero delay the autocorrelation signal, being a coherent superposition of the electric field from each arm, gets its peak value

$$A_2(\tau = 0) = 16 \int A^4(t) dt. \tag{2.140}$$

At the next delay of one-half light period, the two fields add with opposite phase, resulting in a near zero signal. For large delay compared to the pulse duration, the envelopes of the constructive and destructive will merge into the intensity autocorrelation, which reads

$$A_2(\tau \to \infty) = 2 \int A^4(t) dt. \tag{2.141}$$

In this case, the interferometric autocorrelation is said to has a peak to back ground of 8 to 1. Because of its dependence on the fourth power of the fields combining in phase, the interferometric autocorrelation trace is more sensitive to the pulse shape than the intensity autocorrelation.

In most practical cases of interest, the second and third terms in the expansion (2.136) can be neglected by using, for instance, suitable glass filters. The interferometric autocorrelation reduces then to the sum of background term and the intensity autocorrelation (2.127). As a result, $A_2(0) = K_0(0) = 6\int A^4(t)dt$, and the peak to background is 3 to 1. The function (2.137) is generally called the intensity autocorrelation with background.

The third term (2.139) is a autocorrelation of the SH field. In the absence of phase modulation, $\partial^2\varphi/\partial t^2 = 0$, this function is identical to the intensity autocorrelation. This property has been successfully exploited to study the phase modulation of ultrashort laser pulse [46].

For more details, the interferometric autocorrelation of a linearly Gaussian-chirped pulse (2.25) will be considered. Here, for convenient reason, the field amplitude is assumed to be unit. The interferometric autocorrelation now becomes

$$\begin{aligned} A_2(\tau) &= \left[1 + 2e^{-\tau^2/\tau_G^2} + 4e^{-(3+\alpha^2)\tau^2/4\tau_G^2}\cos\frac{\alpha\tau^2}{2\tau_G^2}\cos\omega_l\tau\right. \\ &+ \left. 2e^{-(1+\alpha^2)\tau^2/\tau_G^2}\cos 2\omega_l\tau\right] \end{aligned} \tag{2.142}$$

Replacing $\omega_l\tau$ by π and 2π in (2.142), one can respectively obtain the upper and lower envelopes. Fig. 2.10 shows the interferometric autocorrelation traces and the intensity autocorrelations with background for the cases of gaussian pulses without chirp ($\alpha = 0$) (Fig. 2.10.a) and with various chirp parameters (Fig. 2.10.b). As discussed in [47], the lower envelope has a maximum at $\tau = \tau_c$, which is found by setting the first derivative of the equation for lower envelope to zero.

As α is increased, this maximum moves toward zero delay along a curve close to the intensity autocorrelation. For $\alpha \gg 1$, the pulse front and pulse tail are no longer coherent with each other and the envelopes of the interferometric autocorrelation merge with the intensity autocorrelation for $\tau > \tau_c$. So by identifying the measured autocorrelation with Fig. 2.10.b, one can measure the pulse duration as well as the chirp parameter α (from the height of the lower envelope maxima).

The interferometric autocorrelation discussed above is one of the first phase-sensitive correlations used to study the shape of ultrashort laser pulses. It, however, can only qualitatively test the presence and type of phase modulation and quantitatively measure a linear chirp. Nevertheless, it has been proven to be the standard technique,

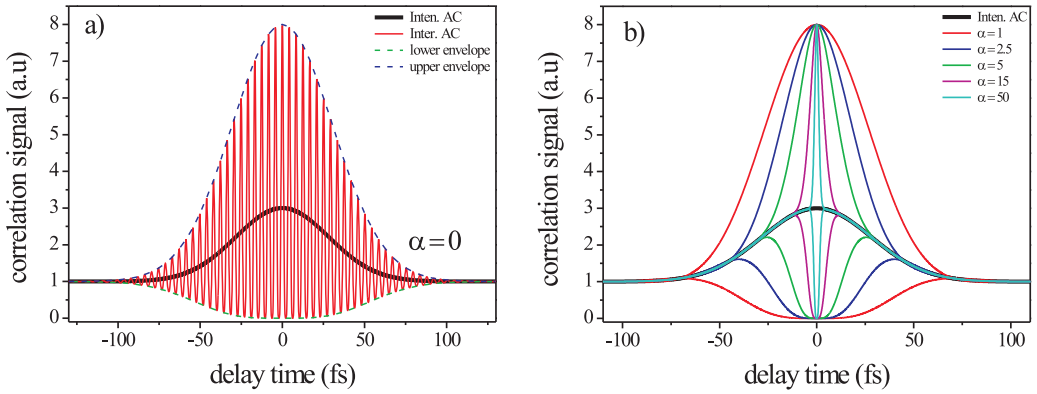

Fig. 2.10: The interferometric autocorrelation traces of Gaussian pulses: a) without chirp and b) for various values of linear chirp parameter. In graph b), the appropriate lower and upper envelopes are plotted with the same color and separated by the intensity autocorrelation, which is independent on chirp (Inten. AC: the intensity autocorrelation; Inter. AC: the interferometric autocorrelation). For more explanations, see text.

which is usually used to check out the accuracy of a new proposed correlator.
To date, one can also fully characterize ultrashort laser pulses by applying some useful methods such as FROG (**F**requency-**R**esolved **O**ptical **G**ating) [48], SPIDER (**S**pectral **P**hase **I**nterferometry for **D**irect **E**lectric-field **R**econstruction) [49], and PICASO (**P**hase and **I**ntensity from **C**ross-correlation **A**nd **S**pectrum **O**nly) [50]. Generally, all of the techniques must use a suitable iterative algorithm to retrieve spectral phase from measured data. From this point of view, PICASO technique is more favored because of its rapidity. FROG, however, is the most widely used and powerful technique, and has become commercially available. To study these themes in details is beyond the scope of this work. For more discussions, see the references given above.

Chapter 3

The High Dynamic Range Third Order Correlator

As discussed in chapter 1, it is essential to monitor the pre-pulses and pedestals in laser-matter interaction experiments. In such experiments, if the temporal range of interest is about several hundred picoseconds, the third-order correlation is obviously the choice. In this chapter, the principles and experimental set up of a **H**igh **D**ynamic **R**ange **T**hird-Order **C**orrelator (HDRTC) will be discussed. The femtosecond laser system used in this work is also briefly described.

3.1 Principles

Third-order correlation technique based on three-photon absorption has been realized by Langlois *et al.* [51]. The method has been proven to be simple and sensitive. However, this kind of correlator shows a short usable scan range ($\sim$ 1 ps) and wavelength region from 1.4 to 1.6 μm, which does not satisfy the requirements of laser pulses in many experiments.

Third-order correlation is also possible using four-wave mixing (FWM) and has been published elsewhere. Because of being the third-order nonlinear effect, the process has very low conversion efficiency and therefore will not be suitable for the purpose of building a high-dynamic range correlator.

In this work, the third-order correlator relies on the third-harmonic generation requiring two BBO-crystal plates in series, a doubling crystal (doubler) followed by a tripling one (tripler). The second-harmonic 2ω is first generated in the doubler using SHG-type I (ooe), and then is mixed with the remnant first-harmonic ω in the tripler to produce the third-harmonic 3ω by exploiting the SFG-type II (oee) process. This setup configuration has many advantages compared with the previously mentioned systems. Firstly, by using only second-order nonlinear effects, one

gets stronger harmonic signals. Secondly, the interplay between type I-II processes makes it easier to implement the experiments. In addition, the conversion efficiency is thereby automatically increased - one needs not use an extra $\lambda/2$-plate to drive the polarizations of the harmonic pulses to achieve phase-matching.
In the third-order correlator, the second-harmonic pulse $I^2(t)$ and the fundamental pulse $I(t)$ are correlated with each other by varying the degree of temporal overlap between them in the tripler. The normalized third-order intensity correlation can be directly obtained by substituting $n = 2$ in Eq.(2.134)

$$A_3(\tau) = \frac{\int I(t+\tau)I^2(t)dt}{\int I^3(t)dt}. \tag{3.1}$$

By using any correlation technique, the pulse shape must usually be presumed. And, as referred to previously, the pulse duration will sensitively depend on the assumed pulse shape. The third-order correlation functions and their appropriate FWHMs for some useful pulse shapes are listed in Table 3.1.

Pulse shape	Third-order Correlation $A_3(\tau)$	τ_{3p}/τ_p
Gaussian $I(t) = e^{-t^2/T^2}$ $\tau_p = [2\sqrt{\ln 2}]T$	$e^{-2\tau^2/3T^2}$	1.22
Hyperbolic secant square $I(t) = \mathrm{sech}^2(\tau/T)$ $\tau_p = [2\ln(\sqrt{2}+1)]T$	$\frac{5}{2}\frac{\sinh(\tau/T)\cosh(\tau/T)^2 + 2\sinh(\tau/T) - 3\frac{\tau}{T}\cosh(\tau/T)}{\sinh(\tau/T)[\cosh(\tau/T)-1]^2[\cosh(\tau/T)+1]^2}$	1.29
Exponential $I(t) = e^{-\lvert t/T\rvert}$ $\tau_p = [2\ln 2]T$	$2e^{-\lvert\tau/T\rvert} - e^{-\lvert 2\tau/T\rvert}$	1.77

Table 3.1: The third-order correlation functions for some useful pulse shapes (τ_p: FWHM of the fundamental pulse, τ_{3p}: FWHM of the correlation function, T: constant) [25].

Before moving to the experiment setup of the HDRTC, we would like here to analyze the problems around its "high-dynamic range", which play the decisive role in designing the correlator.
In this work, noise can be reduced to the order of $10^{-3} - 10^{-4}$ through averaging

the correlation signal many times[1], using the Trigger technique in combination with **S**ample-**A**nd-**H**old (S&H) box and taking into account the scattering problems of laser pulses on the nonlinear crystals. Now, the remaining problem is how to generate the maximum THG signal at zero delay. From the theory of SFM process discussed previously, the harmonic (SH or TH) signal becomes stronger by increasing the intensity of the incident waves. However, in the case of a third-order correlator, this is not always the advantage. The two pulses can only be correctly correlated when the nonlinear crystals acts in such a way that the generated harmonic signal is a product of the intensities of the two incident pulses. In other words, in order for the theory of third-order correlation to be true, the conditions of UPA by SHG and THG processes must be satisfied. In addition, when the intensities are too high, the nonlinear processes become saturated and, as the result, the correlation measurements show longer pulse durations.

The other difficulty appears when one just thinks of applying thick nonlinear crystals for more conversion efficiency. Because of the sinc^2-dependence on the phase-mismatch δk (2.77), the conversion efficiency of the harmonic generation is only considerable for $\delta k = 0$, or in other words, the case of perfect phase-matching. However, the ultrashort laser pulses have a very broad bandwidth. For instance, a 100 fs laser pulse with cavity length of 1 m has a spectral bandwidth $\triangle\nu \approx 10^{13}$Hz equivalent to about 10^5 longitudinal modes. And thus the phase-matching condition can never be fulfilled for all the frequency components, especially in thick nonlinear crystals. In addition, in such dispersive media and even in the case of absolute phase-matching, the group velocity-mismatch also causes inefficient harmonic-conversion, as directly seen from (2.99). Moreover, here plays the GVD an important role in deforming the pulses as well. It causes the pulse broadening, and as the result, leads to an inaccurate correlation measurements.

To overcome the problem of phase-matching in thick nonlinear crystal, the method of using an angle-dithered nonlinear crystal has been recently reported [52]. It has been shown that the phase-matching bandwidth needs not exceed the pulse bandwidth on every pulse, but only the phase-matching bandwidth integrated over the measurement period does need. This condition can be achieved by, because of the sensitive dependence on angle of the range of wavelengths, angle-dithering the nonlinear crystal. The technique shows greater signal strength, removes the phase- and group velocity-mismatch effects. The perturbation of the GVD effect, however, stays unsolved.

In ultrashort laser pulse measurements, it is usually recommended to use thin nonlinear crystal, specially when the laser intensity is sufficiently high. For example, it

[1]From the practical point of view, it does not take much time by 1kHz laser systems.

has been shown that for lasers with pulse duration in the sub-10-fs range the crystal thickness should not exceed 25 μm [4, 53]. In such a crystal, the nonlinear effects referred to above in this section are practically negligible.
The last but not least problem is how to wisely record the correlation signal. Because of being the most sensitive, broadband, and very fast detectors, photomultipliers (PMTs) are most widely used in measuring ultrashort laser pulses. However, even the best PMTs have the dynamic range[2] of only $10^3 - 10^4$ while the dynamic range of the correlators is usually required to be of about $10^6 - 10^8$ or even higher, depending on the requirements of appropriate experiments. Indeed, for typical ultrashort laser pulses, the THG-signal usually decreases when the delay between the incident waves become larger. Employing this fact, one can always operate so that the THG-signal lies in the valid response region of the detector (Fig. 4.2.b). In order to do so, one can vary either the intensities of the laser pulses in front of the tripler or the THG-signal before it goes into the detector (for instance of using neutral density filters), or both of them. The former is chosen in this work for practical reasons: the experiment setup is simpler and because of the sensitive relationship between TH and fundamental intensities: $I_{3\omega}(t) \sim I^3_{\omega}(t)$, it spares much time doing experiments.

3.2 Experimental Setup

3.2.1 The 1 kHz-Laser System

The 1 kHz-laser system is designed by the Quantronix firm to upgrade the ultrashort laser system of 1 mJ energy levels up to 5 mJ at 1 kHz repetition rate in the near infrared region of the spectrum. It consists of three main elements[3]:

- The Ti:sapphire Mira-oscillator
- The 8-path Odin-amplifier system
- The 3-path MPA-amplifier system

The schematic of the fs-laser system is shown in figure 3.1. The Ti:sapphire oscillator works with configuration described in the section of the generation of ultrashort pulses (Fig. 2.1) and has a repetition rate of 81 MHz. The laser pulse generated by this system has a energy of about 6 nJ and a 28 nm bandwidth (FWHM). The pulse duration from the Oscillator is about 60 fs[4].

[2] By the dynamic range of a detector we mean the ratio of the maximum to the minimum value of its linear response range.

[3] The 50fs-1kHz-1mJ Odin-amplifier system is also described in the works of Hacker [54] and Stobrawa [55].

[4] This laser pulse is not Fourier-transmitted because of the intracavity dispersion materials, specially by the output-window of the oscillator.

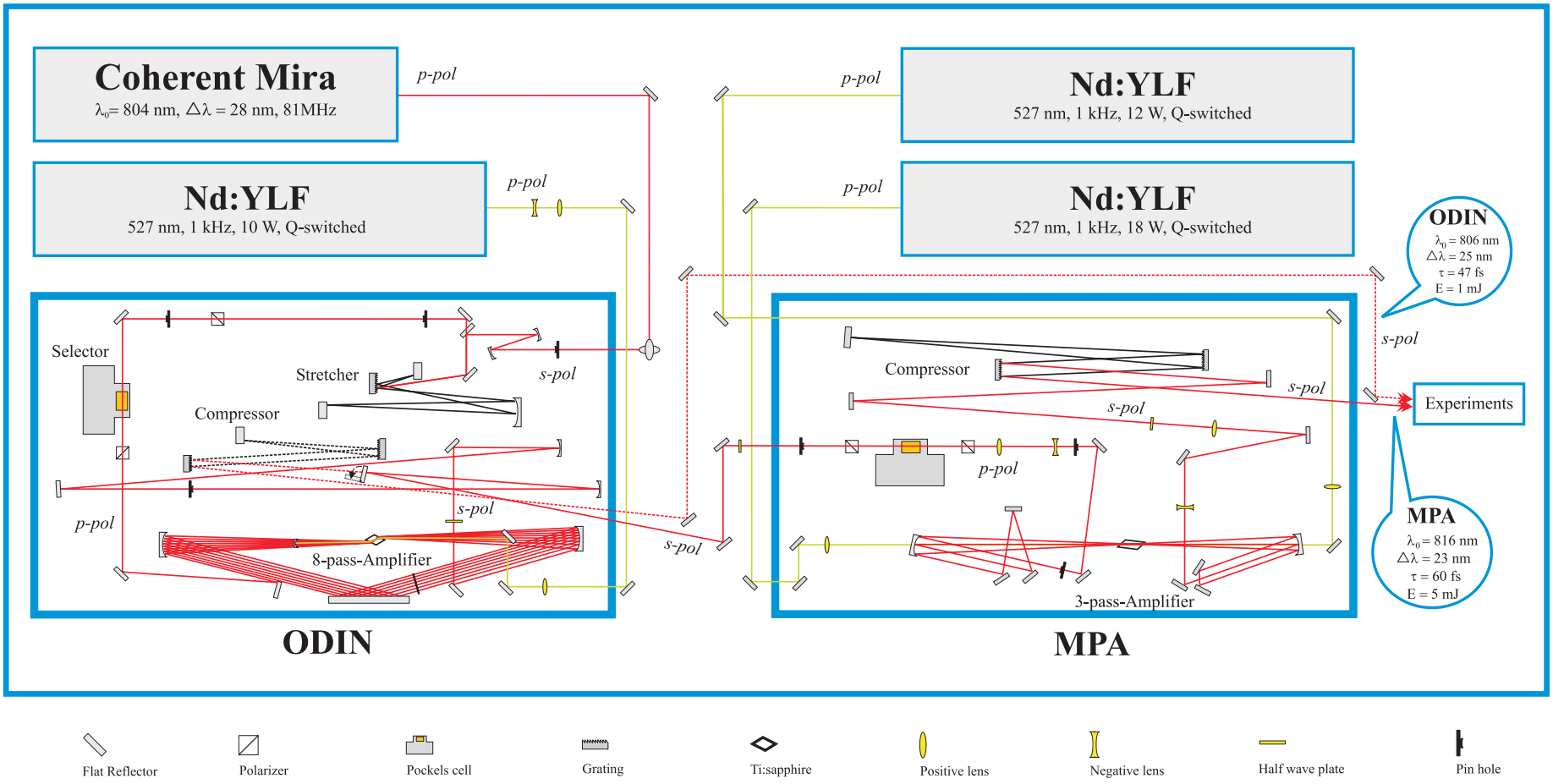

Fig. 3.1: The schematic of the 1 kHz ultrashort laser system

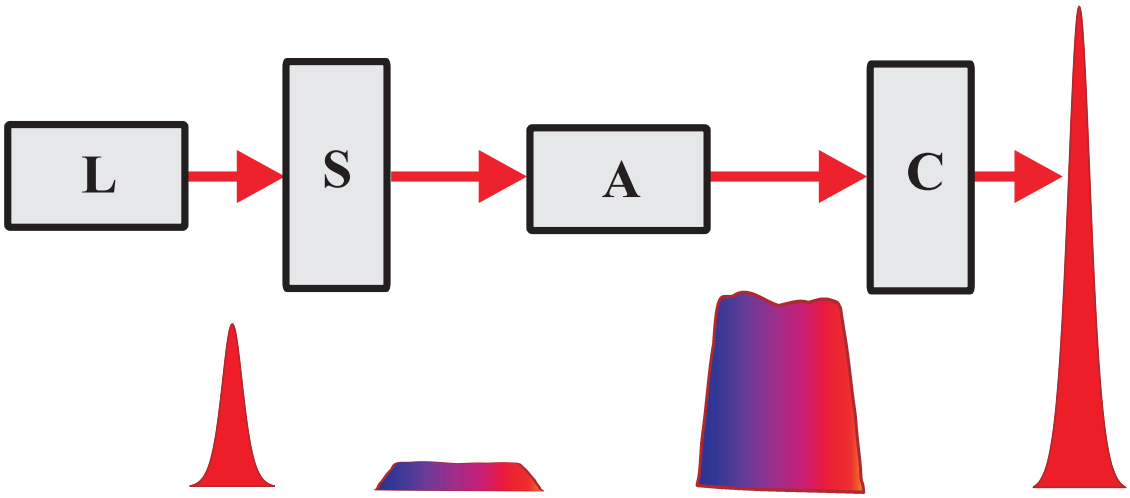

Fig. 3.2: The principle of the Chirped-Pulse-Amplification technique. A short laser pulse with low energy level is initially chirped and stretched in an optical stretcher S. After stretched, it has relatively low peak power and can be amplified to saturation in an amplifier A. An optical compressor C is then used to restore the original short pulse duration, producing a ultrashort optical pulse with large energy.

The seed laser pulse is then in turn amplified by the Odin-and MPA amplifier systems using the CPA[5]- technology [6]. The CPA technique (Fig. 3.2) is utilized here in order to eliminate high peak power in the amplifier chain, which could lead to damage of the optical components and mirror coatings, and avoid the unexpected nonlinear effects. Accordingly, the seed laser pulse width is temporally stretched to $\sim$ 30 ps in a so-called optical stretcher, which allows different components of the spectrum to travel through different optical paths. By a pulse picker, comprised of a Pockels cell and two polarizers, the seed pulse at 81 MHz repetition rate is selected to 1 kHz and then injected into Ti:sapphire as the active medium for amplification. After travelling 8 paths through the Ti:sapphire crystal the seed laser pulse is amplified to about 1.5 mJ. The pump laser used in this system is Q-switched diode-pumped Nd:YLF laser at 527 nm central wavelength. It has a 1 kHz repetition rate, 10 mJ pulse energy and pulse duration of about 250 ns.

At this stage, the amplified laser pulse can be either compressed by the pulse compressor in the Odin-amplifier system or sent to MPA system for further amplification. In the former case[6], the laser pulse after compressed has a energy of $\sim$ 1 mJ, 25 nm

[5] **C**hirped **P**ulse **A**mplification.

[6] This case is also referred to since the MPA-amplifier system sometime had technical problems and the experiments must be accomplished with the laser from Odin-amplifier system.

Parameters	Mira-oscillator	Odin-amplifier	MPA-amplifier
Pulse energy	6 nJ	1 mJ	5 mJ
Repetition rate	81 MHz	1 kHz	1 kHz
Central wavelength	804 nm	806 nm	816 nm
Bandwidth	28 nm	25 nm	23 nm
Pulse duration	60 fs	47 fs	60 fs

Table 3.2: The parameters of the fs-laser system

bandwidth and 47 fs pulse duration. In the latter case, similar to that described in the Odin-amplifier system, the seed laser pulse travels three times through the Ti:sapphire crystal and is amplified to ~ 6.3 mJ. After compression, it has an energy of 5 mJ with 23 nm bandwidth and pulse duration of about 60 fs. The pump lasers used in MPA-system are also Nd:YLF lasers with total pulse energy of 30 mJ. Table 3.2 summarizes again the parameters of the fs-laser system.

3.2.2 The High-Dynamic Range Third-Order Correlator

We now proceed to describe the experimental setup of the high-dynamic range third-order correlator schematically shown in Fig. 3.3. The correlator is comprised of three main parts:

- The intensity attenuator
- The harmonic generators: the doubler and the tripler
- The detector

The ultrashort laser pulse with *s-pol* coming from Odin-MPA amplifier system is first attenuated and driven by the intensity attenuator and then injected to the doubler (BBO, 100 μm) to produce SH radiation (Type I: $o+o \rightarrow e$). After leaving the doubler, the generated SH and fundamental signals are split by a 1 mm-thick dichroic mirror DM (OIB[7] Jena), which is high-reflecting at 400 nm and high-transmitting at 800 nm central wavelength with AR-coating for 800nm at the backside, and travel along different optical paths with help of the appropriate broadband mirrors.
The ω-beam is further attenuated by a substrat (Quartz) to reduce the unexpected scattering signals and avoid the saturation in the tripler. The curved, aluminium-coated mirror with the focal length of 20cm is used to physically overlap the two laser pulses in the tripler (BBO, 100 μm) to generate 3ω-radiation (Type II: $e+o \rightarrow e$). The temporally overlapping degree of the pulses can be varied by changing the optical path of the 2ω-pulse with the help of a stepping motor (OWIS, SM30), which is

[7] Stands for ***O**ptische **I**nterferenz **B**auelemente*.

driven by a computer. The computer-simulation with Lab2 [56] shows that in this case the phase-matching condition is only possible for SHG being *o*-pulse. As the result, the 3ω-pulse has s-polarization, the same as that of ω-pulse. The polarization of interacting pulses can be seen in Fig. 3.3.

To increase the signal-to-noise ratio, some special techniques have been applied in

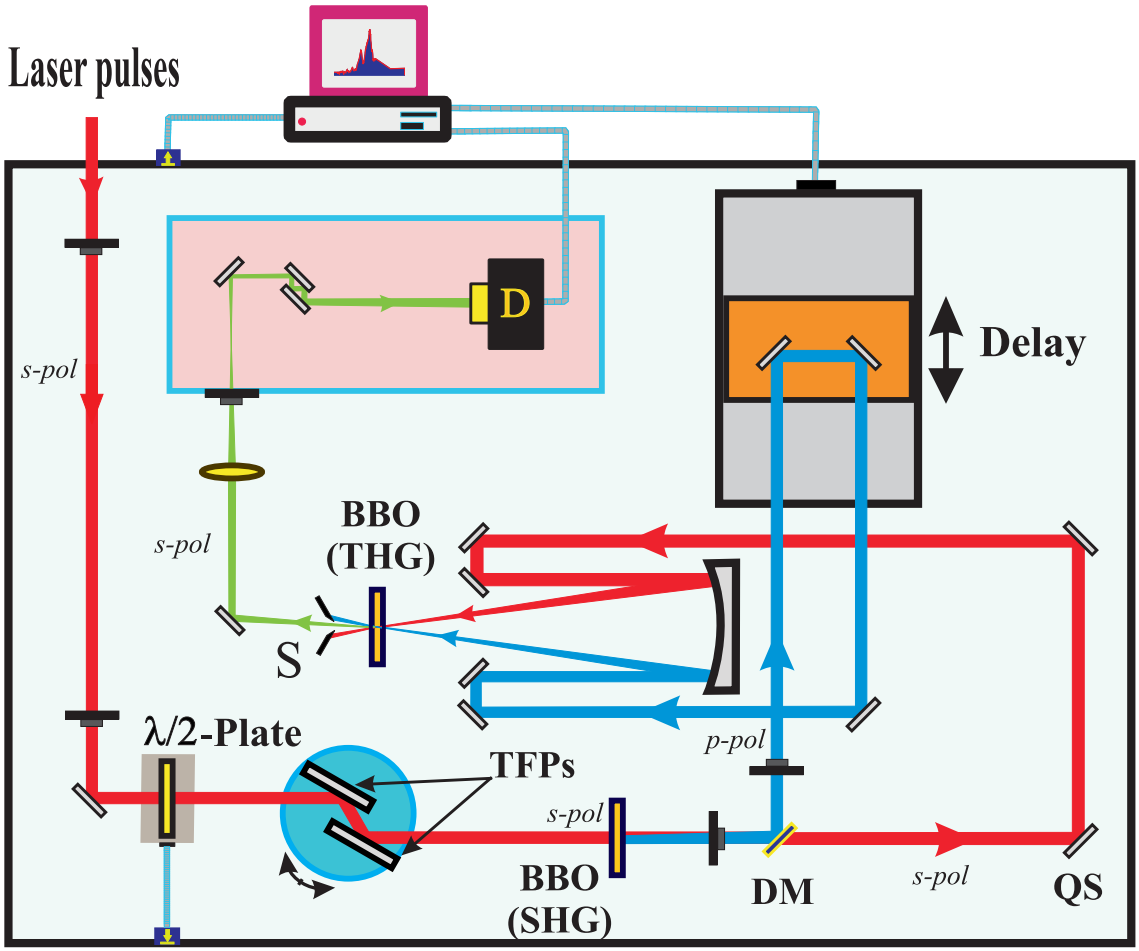

Fig. 3.3: The schematic of the high-dynamic range third-order correlator(TFPs: the thin film plates, DM: the dichroic mirror, QS: Quartz substrat; S: the after-crystal slit).

this work.

Firstly, the after-crystal slit S made of two razor blades is installed to stop the residual ω and 2ω-beams from going into the detector, and more important, to reduce the 3ω-radiation generated by scattering of the ω-pulse alone at the front surface of the tripler. This 3ω-light can propagate in every direction and may reach the detector, producing the delay-independent background. The slit is therefore placed as near the crystal as possible. The razor blades are constructed at an suitable angle with each other that minimizes the design and prevents the ω-pulse from being backwardly reflected, which may introduce additional background. Further reduction of this kind of background can be achieved by carefully programming with LabView.

Secondly, the third-harmonic beam after the slit is focused into a box through a pinhole, which separates the detector from scattered signals coming from other directions. Before arriving the detector, the 3ω-signal is "cleaned" by a so-called 3ω-*reflecting filter*, which is comprised of two broadband mirrors for 266 nm central wavelength positioned parallel to each other. The beam is reflected back and forth about 10 times or more. This design has an additional advantage that because of the multi-reflection on the mirrors, only the signal with certain direction can reach the small window of the detector.
The third-order correlation trace (correlation function) versus delay is then read by the detector and through the S&H box analyzed by the computer.
In what follows, the setup of the HDRTC with the main elements will be described in more detail, and the measured data and appropriate evaluations will be given. The problems emerging in the experiments and their solutions are also discussed.

Chapter 4

The Experiment Results

4.1 The Intensity Attenuator

The **I**ntensity **A**ttenuator (IA) consists of a 2.5 mm-thick halfwave plate[1] and a pair of broadband (700-900 nm) **T**hin **F**ilm **P**lates[2], which are constructed parallel with each other. This configuration allows the light wave, which falls onto one TFP, to leave the other in the parallel direction. Moreover, if the incident angle is equal to the Brewster-angle of the TFP [30], the reflected wave is linearly polarized with the polarization normal to the incident plane (*s-pol*) or in other words, the TFP acts as a *broadband* **R**eflecting **P**olarizer (RP). Normally, it is already enough to use just one TFP for the IA [57]. However, with the reflectivity $R_s \approx 62\%$ and $R_p \approx 0.2\%$ respectively for *s-pol* and *p-pol* at the Brewster-angle, the configuration of the two parallel TFPs makes it easier for experiment alignments and offers higher contrast.

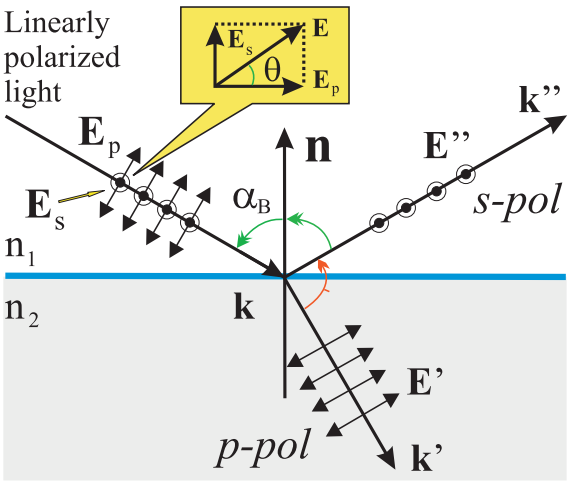

Fig. 4.1: The reflection and transmittance of linearly polarized light at Brewster-angle.

Assuming the incident wave with intensity I_i is linearly polarized and the polariza-

[1] Linos Photonics/362701244.
[2] TFPs, Layertec/999999.

tion vector is made an angle θ with the incident plane as shown in the Fig. 4.1. The intensity of the reflected wave coming at the Brewster-angle can be simply given as:

$$I_r = R_{s1} R_{s2} I_i \sin^2 \theta, \tag{4.1}$$

where R_{s1}, R_{s2} are the reflectivity coefficients of the *s-pol* components of light on the first and second TFPs, respectively. The equation (4.1) implies a method to drive the intensity of reflected light by changing the angle θ. This can be done with a $\lambda/2$-plate in complication with a rotating motor[3]. The characteristic curve of the polarizer is theoretically and experimentally shown in Fig. 4.2. From the experi-

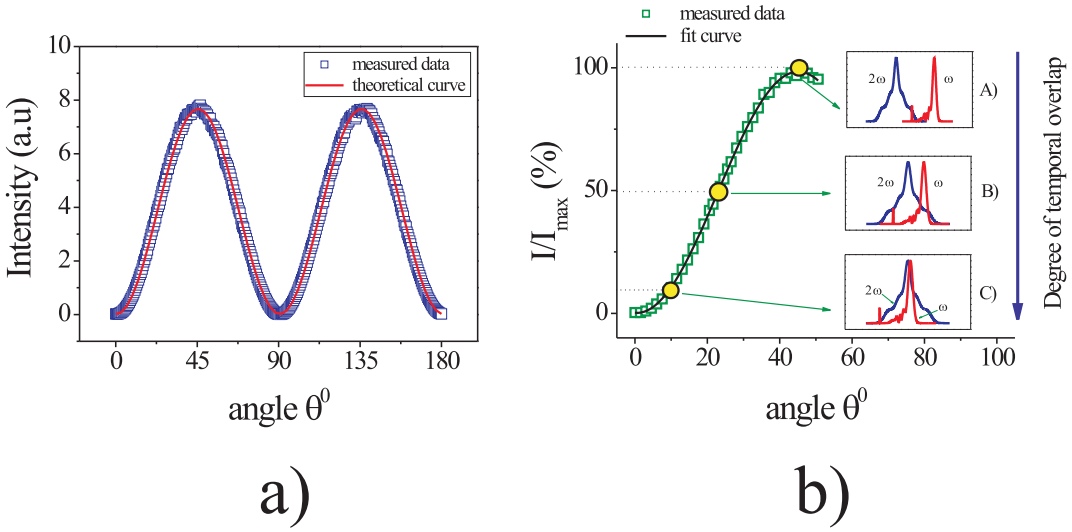

Fig. 4.2: a) The dependence of reflected laser intensity on polarization angle θ; b) The principle of using IA to drive the THG signal so that it always lies in the linear response range of the detector (I: intensity of laser pulse leaving from IA and being function of angle θ; I_{max}: the maximum value of intensity I). The IA works at various stages of intensity. At large delay A), the IA works at first stage, where the laser pulse leaves it with I_{max} (100%). And at near-zero delay, B) or C), where the THG-radiation is strong, the IA works at lower stages of intensity, for instance, 50% or 10%, respectively.

mental point of view, even at angle $\theta = 0^0$ the laser intensity leaving from the RP actually has a nonzero value, what is unexpected from (4.1). The reasons for this fact may be given as the followings.

Firstly, the Eq.(4.1) is only satisfied for monochromatic wave at a certain wavelength. In the case of ultrashort laser pulses, it is implied to be true for the central wavelength. And therefore, at the Brewster-angle of this central wavelength, the *p-pol* component of the other wavelengths still exists and contributes to the nonzero part of the reflected light. By using the Lab2-pack [56], one can estimate that the error caused by this process is of the order of about 10^{-3}.

[3]OWIS, DMT 40

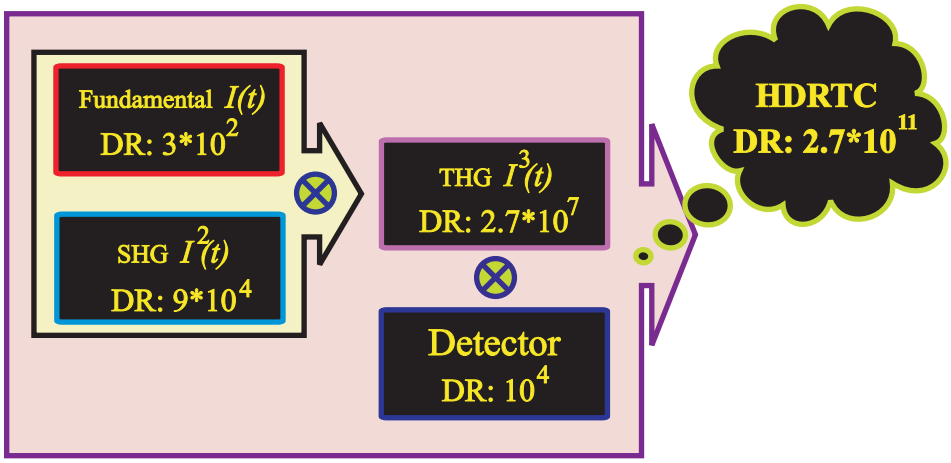

Fig. 4.3: The theoretical dynamic range of the HDRTC (DR: Dynamic Range).

Secondly, because of the technical limits, the error by determining the Brewster-angle for the TFPs is about $\pm 2^0$, within which the measured intensity show a minimum value of the order of 10^{-2} and stays the same for all angles. In effect, the contrast[4] of the polarizer, defined as the ratio of the maximum and minimum intensity I_r, is of about $2 \times 10^2 - 3 \times 10^2$. On this occasion we can roughly estimate, with this intensity attenuator how far we can hope to achieve the high-dynamic range of the correlator. The schematic diagram is shown in figure 4.3. With the assumption that the detector has a dynamics of 10^4, we receive the theoretical dynamic range of 10^{11}. It will be clear later, in which case it is possible to achieve this level.

4.2 The Harmonic Generators

The nonlinear crystals used in this work are the **B**eta **B**arium **B**orate or BBO crystals. The BBO crystal is a trigonal negative uniaxial crystal and combines a number of unique properties. These properties include wide transparency and phase matching ranges, large nonlinear coefficient (about 6 times more than that of KDP[5]-crystal), high damage threshold and excellent optical homogeneity. Therefore, BBO provides an attractive solution for various nonlinear optical applications, especially in ultrashort laser pulse measurements. Some important properties of BBO- crystals are shown in the table 4.1. The BBO crystals used are provided with p-coatings[6] to prevent the polished surfaces of BBO from exposure to moisture. This increases the conversion efficiency, but still has some inconveniences, as shown later.
The main disadvantage when using a BBO crystal is that BBO has a small ac-

[4] Also called the dynamics of the intensity attenuator.
[5] **P**otassium**D**ihydrogen-**P**hosphate
[6] Protective coatings.

β-BaB_2O_4	
Transmission range:	190 - 3500 nm
Phase-matching range:	189 - 1750 nm
Optical damage threshold:	10 GW/cm^2 (100 ps-1064 nm)
Optical homogeneity:	$dn \approx 10^{-6}\text{cm}^{-1}$
Therm-Optic coefficients:	$dn_0/dT = -9.3 \times 10^{-6}/^0C$ $dn_e/dT = -16.6 \times 10^{-6}/^0C$
Phase-matching angles: SHG: 800 $\rightarrow$ 400 nm SFM: 800 + 400 $\rightarrow$ 266.6 nm	 $\theta_m = 29.2^0, \quad \phi = 0^0$ $\theta_m = 55.4^0, \quad \phi = 0^0$
Effective nonlinearity coefficients:	$d_{ooe} = d_{31}\sin\theta - d_{22}\cos\theta\sin 3\phi$ $d_{eoe} = d_{oee} = d_{22}\cos^2\theta\cos 3\phi$
Dispersion Relations (λ in μm) $n_o^2(\lambda) = 2.7359 + \frac{0.01878}{\lambda^2 - 0.01822} - 0.01354\lambda^2$ $n_e^2(\lambda) = 2.3753 + \frac{0.01224}{\lambda^2 - 0.01667} - 0.01516\lambda^2$	

Table 4.1: The main properties of BBO used in this work.

ceptance angle ($\sim$ 1 mrad) and relatively large walk-off angle ($\sim$ 55 mrad), which limits the harmonic conversion efficiency. Therefore, an input laser radiation with good beam quality and low divergence is required. In this work, to reduce these limitations and to increase the signal-to-noise ratio, the input laser beam at SHG-crystal is therefore not focused. Since the input laser beam from the MPA-system is relatively large ($\sim 6mm$ diameter) while the useful surface of the doubler has a diameter of $3-4$ mm, it is suggested to use an appropriate reflecting broadband telescope to increase the intensity of the input wave for more conversion efficiency. The use of a transmitting telescope (for instance with lenses) will introduce, besides causing the group velocity dispersion, the tilt of pulse front with respect to the phase front leading also to increasing delay across the beam [35]. And as the result, the measured correlation shows longer pulse duration.

4.3 HDRTC with the SiC detector

The detector used in this work to realize the 3ω-radiation is a SiC detector with pre-amplifier. The calibration of its sensitivity with respect to the 3ω-radiation can be seen in figure 4.4. The measurement shows a *realizable* dynamics of the detector of about 10^4. The word "realizable" here is related to the limitation of the S&H box. Its solution is about 10^{-4} input signal (usually of order 1 V).
As discussed previously, the validity of the UPA is necessary for the theory of the

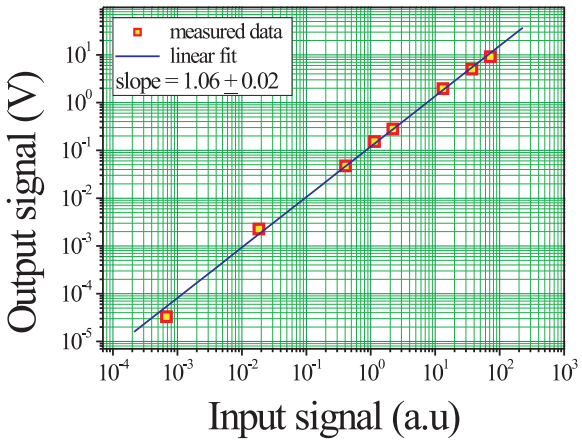

Fig. 4.4: The calibration of the SiC photodiode for THG-signal

third-order correlator. Correspondingly, the following relations

$$\text{SHG}: \quad I_{2\omega} \sim I_{\omega}^2 \tag{4.2}$$

$$\text{THG}: \quad I_{3\omega} \sim I_{\omega} \cdot I_{2\omega} \sim I_{\omega}^3, \tag{4.3}$$

must be experimentally realized and are shown in figure 4.5.

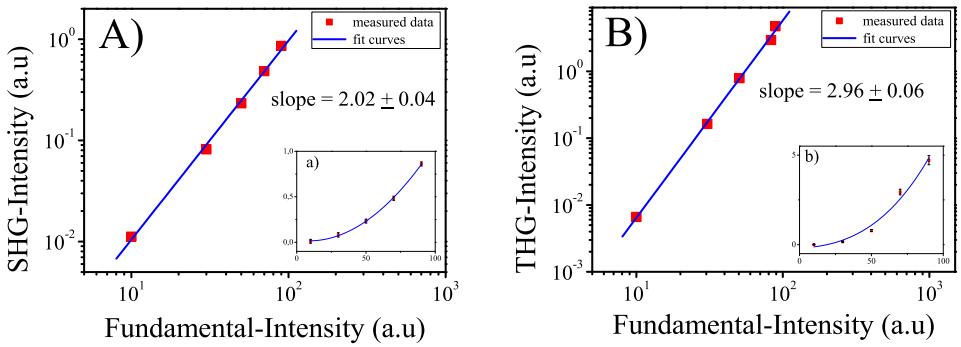

Fig. 4.5: The tests for the validity of the UPA. The SHG intensity depends quadratically on fundamental intensity: in log-scale (A)) and in linear-scale (a)). The THG-intensity shows cubic dependence on fundamental intensity: in log-scale (B)) and in linear-scale (b)).

It is also very important to make sure that the spectrum with broad bandwidth of the input laser pulse must be approximately maintained while travelling through the optical components of the correlator. For this purpose, the spectra of the input

laser pulse and the ω-pulse in front of the tripler are measured and shown in figure 4.6. The measurement shows a slightly narrower bandwidth of the spectrum of the ω-laser pulse before focusing compared with that of the input laser pulse. However, the difference can be practically neglected. The Fourier-transmitted pulse duration appropriate to this bandwidth ($\sim$ 22nm) is about 43 fs (for Gaussian-shaped pulse). Figure 4.7 shows the first third-order correlation trace of the HDRTC with a dy-

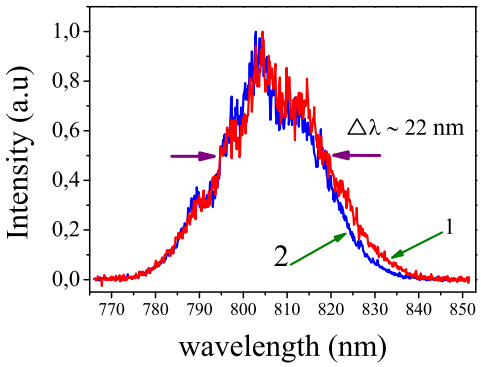

Fig. 4.6: Comparison of the spectra of the input laser pulse (1) and the fundamental pulse in front of the tripler (2).

namic range of 7 orders and a pulse duration of about 80 fs. The measurement was carried out using ultrashort laser pulses from the ODIN-amplifier system. The correlation trace is a asymmetric function of delay time, as expected from a third-order correlator. The measured pulse duration, however, is relatively long compared with

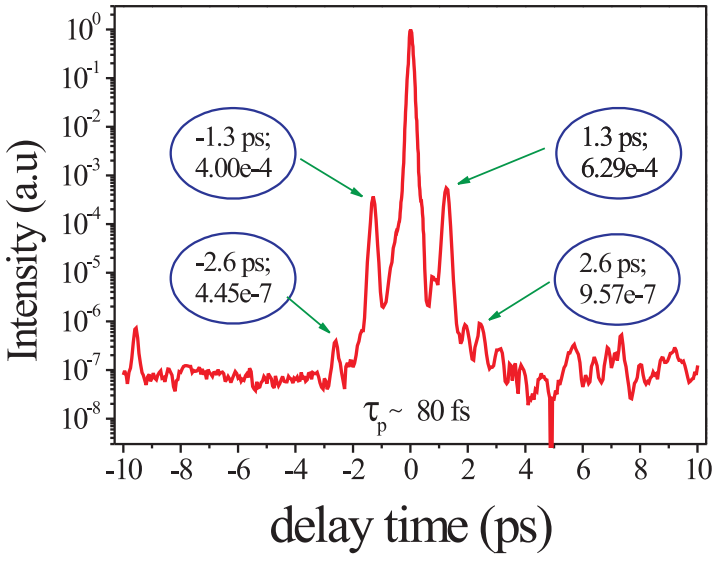

Fig. 4.7: The correlation trace of the HDRTC with SiC-detector.

that of the Fourier-transmitted laser pulse given above. That can be explained by

the presence of chirp coming from the optical stretcher in the Odin-system, which can be totally compensated by the compressor in the MPA-system only, not by the compressor in the Odin-system.
What is unusual also on the Fig. 4.7 is the existence of the pre- and post-pulses (p-pulses), which appear after a time period of about 1.3 ps and show a decreasing amplitude with increasing delay to the main pulse. The intensity ratio between the successive p-pulses is about 10^{-3}. Moreover, they have similar shapes as that of the main pulse. The question now is where they do come from: *from the laser system or from the HDRTC itself?*

4.3.1 The p-pulse problem

The widely realized process to generate post-pulses in laser optics is the back and forth reflection of laser pulse when it travels through, for instance, a glass plate. The time period of about 1.3 ps implies a thickness of $\sim 100\ \mu m$ for such a plate, depending also on the incident angle and the refractive index of the material. The

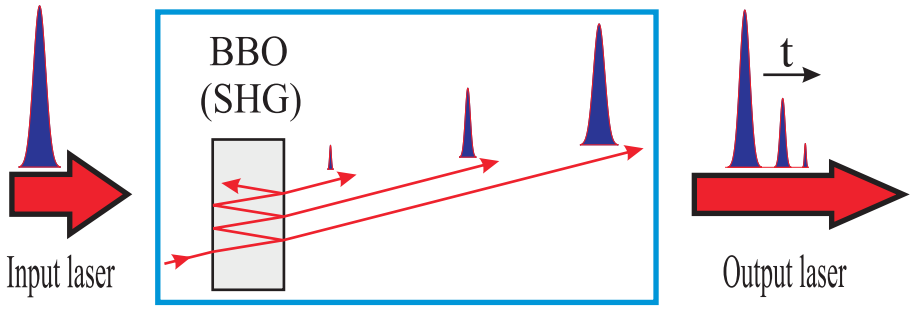

Fig. 4.8: The post-pulse generation of laser pulse because of multi-reflection on BBO crystal's surfaces

doubler (BBO crystal, 100 μm) used in this work has p-coatings, and therefore the back and forth reflection of laser pulse on both surfaces of crystal is possible and illustrated in figure 4.8.
In effect, the ω- and 2ω-pulses when leaving the doubler will have the appropriate post-pulses. The correlation of the main ω-pulse with the post-pulses of the 2ω-pulse will produce the pre-pulses of the THG, and similarly the post-pulses of THG are generated through the correlation of the 2ω-pulse with the post-pulse of the ω-pulse. Figure 4.9 shows the excellent agreement between the simulated and measured third-order correlation functions, where the multi-reflection of the interacting pulses are taken into consideration. The simulation program is written with LabView using Lab2-pack [56] and taking into account the non-zero incident angle, the thickness of the p-coatings, and the different polarizations between the ω- and 2ω-pulses.

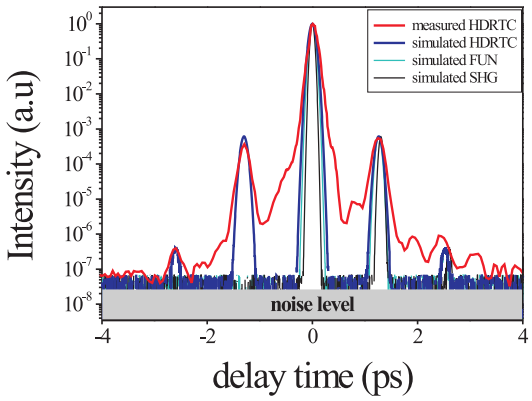

Fig. 4.9: The simulated and measured correlation traces with p-pulses generated by BBO crystal

4.3.2 How to solve the problem?

In fact, the real p-pulses[7] from the laser system may overlap with the p-pulses generated by the doubler (BBO-generated p-pulses) of the correlator and may cause some troubles in characterizing the laser pulse. Therefore, some solutions for this problem should be here discussed[8].

♠ To avoid this problem, it is suggested to use nonlinear crystal with dual-band AR-coatings at 400 nm and 800 nm. In addition to the protective function like that of p-coatings, the AR-coatings help to increase the contrast of the p-pulses to a factor of about $10^5 - 10^6$. In such a case, the first p-pulses in Fig. 4.9 (at delays of about -1.3 ps and 1.3 ps, respectively) have a contrast of about $10^8 - 10^9$ and the problem is practically completely solved.

♠ Indeed, such a replaced AR-coating nonlinear crystal is not always available for different reasons, and hence a simple computer program to analyze the measured data may be useful. From the simulated third-order correlation function, we know relatively well the time period of appearing ($\sim$ 1.3 ps) and the contrasts of the p-pulses. By comparing the measured correlation curve with the simulated curve, we can quantitatively and qualitatively evaluate the possibly real p-pulses which may emerge into the BBO-generated p-pulses.
For a better solution, the main pulse of the measured third-order correlation can be fitted with a widely used pulse shape, for instance, gaussian or sech^2-shape[9].

[7] In most X-ray and plasma experiments, only pre-pulses are of interest.

[8] We would like here to mention that the simple technique using wedge-shaped crystals cannot be applied here to remove the p-pulses problem. Such crystals introduce the tilting of pulse front with respect to the phase front [35], leading to longer measured pulse duration.

[9] For the cases of complex pulse shapes, we refer to iterative fitting technique reported in the work of Naganuma *et al.* [46].

Then, the fitting parameters will be used with the appropriate contrast of the BBO-generated p-pulses to remove them from the measured data. To be able to do so, we have exploited the fact that the post-pulses, generated by multi-reflection of the ω-pulse (or 2ω-pulse also), for instance, on the surfaces of the BBO crystal, and their respective main pulse have a similar temporal shape. As a result, the p-pulses of the third-order correlation also have a similar shape to its main pulse. The accuracy of this method depends strongly on the fitting quality of the chosen pulse shape. Therefore, it is recommended to use for well chirp-compensated laser pulse.

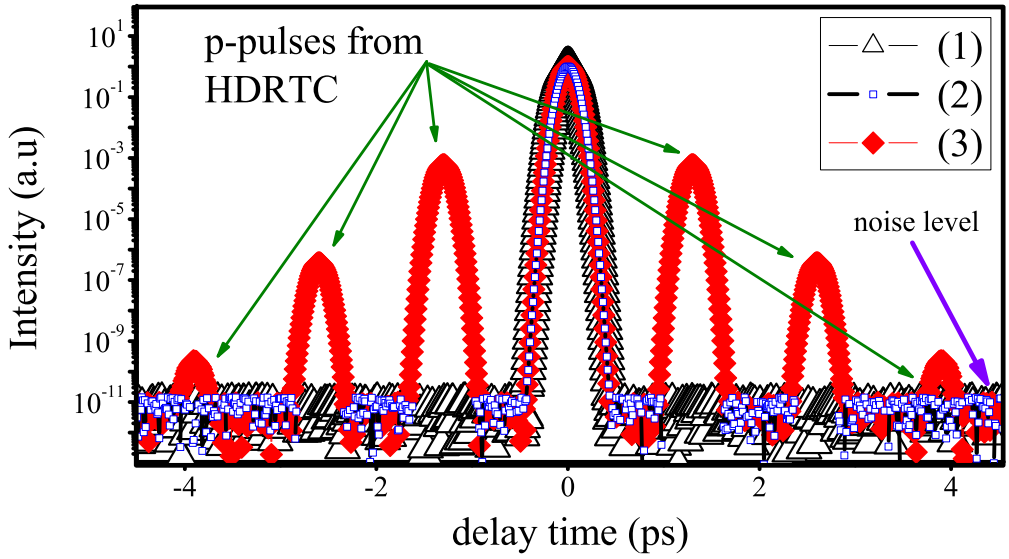

Fig. 4.10: The simulation of modified high-dynamic range third-order correlation to solve the BBO-generated p-pulse problem: 1) the HDRTC-trace of the original Gaussian-shaped pulse; 2) the HDRTC-trace taking into account the multi-reflection of the interacting pulses in the doubler; 3) the modified HDRTC-trace of 2).

To check the idea, the third-order correlations of an original Gaussian-shaped pulse and its respective multi-reflected pulses are simulated and shown in Fig. 4.10. The modified HDR third-order correlation compares relatively well with that of the original pulse.

We have only concentrated on the multi-reflection of the main pulse, which comes from the laser system, and neglected the fact that the pre- and post-pulses of the input laser pulse experience the multi-reflection also, and thereby complicate the third-order correlation (Fig. 4.11). However, with the computer simulation program, we will show that all the BBO-generated p-pulses *concerned this problem*[10] are less

[10]It should be here made clear that there are two types of BBO-generated p-pulses mentioned in

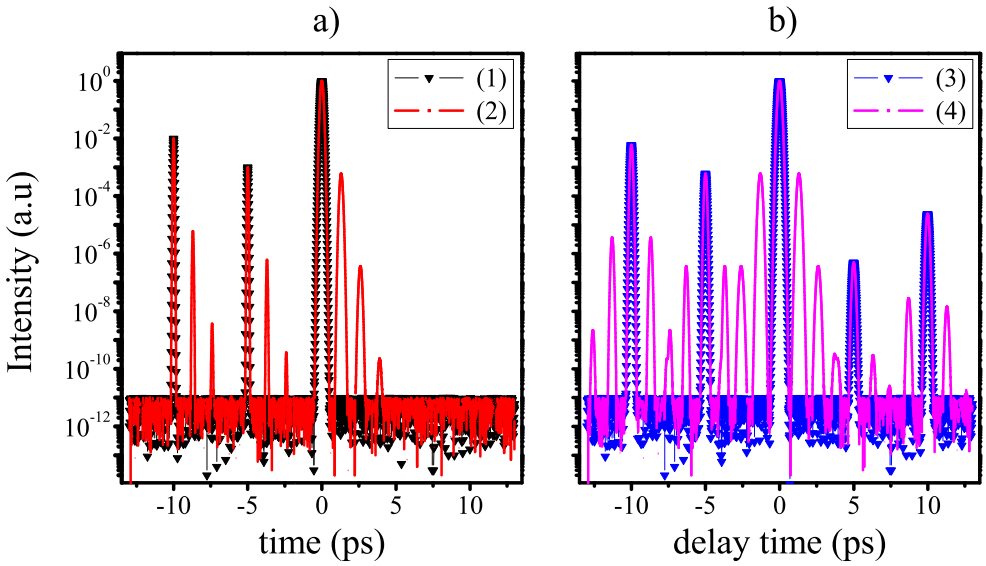

Fig. 4.11: The simulation of the third-order correlation of an input laser pulse with two pre-pulses taking into account the multi-reflections of the interacting pulses on the surfaces of BBO-crystal: (a) - the input laser pulse (1) and the ω-pulse after multi-reflecting (2); (b) - the third-order correlation traces of the input laser pulse without and with multi-reflections (3) and (4), respectively. The graphics show how complicated it could be when the multi-reflections of the pre-pulses of input laser pulse must be considered.

than the interested limit of detection in this work, which is assumed to be about $\sim 10^7$ of contrast.

It can be clearly seen from figure 4.12 that only when the contrast (the inverse quantity of the intensity) of the pre-pulse of the input laser pulse is less than about 2×10^3, the problem involved the BBO-generated p-pulses of type B must be taken into consideration. Nowadays, with help of the Pockel's cell, a commercially available high-intensity laser system can generate laser pulses with contrast (about $10^4 - 10^5$ or more) much higher than the value given above. That means, the effect related to the BBO-generated p-pulses of type B can be practically neglected.

4.3.3 Ultrahigh-dynamic range discussions

The measured correlations showed a dynamic range of about $10^7 - 10^8$, compared to the theoretical value 11 orders of magnitude. In this section, we would like to discuss about the possibility to achieve the theoretical dynamic range and the prob-

this work. The first type (type A) are the p-pulses of the third-order correlation trace generated by the multi-reflections of the main pulses of the ω- and 2ω-pulses only. The second type (type B) are related to the correlation's p-pulses generated by the multi-reflections of the p-pulses of the both ω- and 2ω-pulses. More illustrations can be seen in figure 4.12.

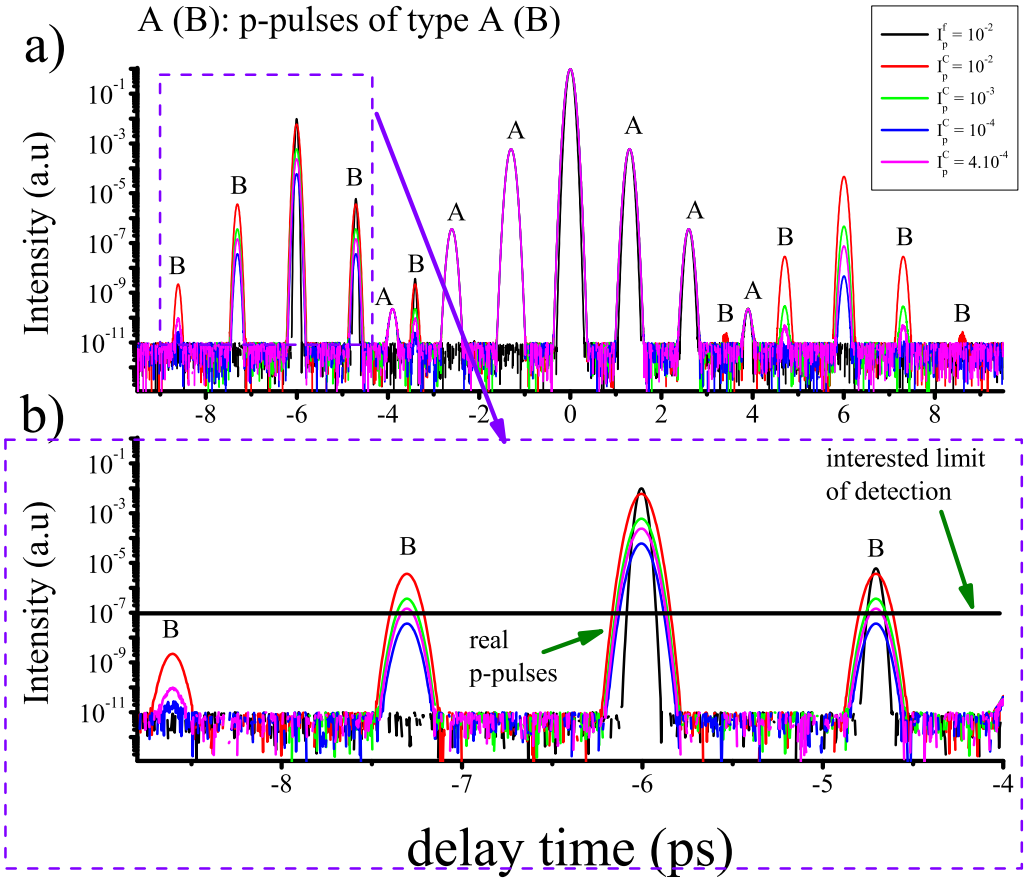

Fig. 4.12: The simulation of third-order correlations with various contrasts of the pre-pulse of an input laser pulse a) and b) - on which the region of the interested pre-pulses is magnified. In principle, both I_p^f and I_p^C imply the intensity of the pre-pulse of the input laser pulse. However, the curve related to I_p^f is the input laser pulse, which is plotted to help to determine the delay time of the "real" p-pulses of the correlation traces; while the other curves, represented by I_p^C, are the third-order correlation traces. The interested limit of detection is determined by the focused intensity of the laser pulse and the optical-breakdown threshold of the target material. See text for the definitions of the p-pulses of type A and type B, respectively.

lem, which may occur by recognized contrast of more than 10^8.

It is realized that higher-dynamic range of the correlator can be achieved by increasing the intensity of input laser pulse. In this work, the intensity attenuator can change the intensity of laser pulse through 7 stages. The principle can be seen in figure 4.2b. The change to the next stage of the IA will change the intensity of 3ω-radiation by about 1 order of magnitude. By working with the SiC detector, the 3 last low-intensity stages cannot be used since at such low intensity levels, the THG-signal is too weak for the detector to detect. That means the used dynamic

range of the IA is lower than the measured shown in Fig. 4.2a ($\sim 3 \times 10^2$), leading to the low-realized dynamic range of the correlator. To be able to receive the theoretical dynamic range value, one can increase the intensity of the input laser[11], as mentioned above, or use a more THG-sensitive detector such as PMT[12]

Even a high intensity-laser pulse with well-compensated phase errors of third- and higher-orders can only reach the contrast ratio of about $10^8 - 10^9$, limited by the pedestal caused by ASE, for example. Moreover, the pulse duration of ASE is in the region of several nanoseconds while the useful temporal scan range of a third-order correlator is just about several hundred picoseconds. So measuring such a laser pulse with a third-order correlator of 10^{11} dynamic range, one will not be able to see the noise-level, what is usual by using third-order correlators with dynamic range lower than the contrast ratio of the laser pulse. To see roughly the noise-level, one can block either the ω- or 2ω-beam (one-beam-blocked noise). The two levels of one-beam-blocked noise should be similar to each other. Otherwise, there may be a problem with scattering of laser pulses in the tripler.

[11] However, one may hit the saturation thresholds in the harmonic generators!

[12] At the beginning, the detector planed to use for this HDRTC was the solar-blind PMT (160-320 nm; Hamamatsu, R7154). Unfortunately, it showed a nonlinear response with respect to 3ω-signal and is under repair.

Summary

The purpose of this work is to build and characterize a high-dynamic range third-order correlator used to characterize the 1 kHz ultrashort laser system. The requirements for the correlator are that it must be sensitive to the temporal asymmetry of ultrashort laser pulses and be able to realize a pulse contrast of more than 10^7. We have proposed an experimental configuration, which promises a theoretical high-dynamic range of about 11 orders of magnitude.

The background information was firstly discussed in chapter 2. The generation, description, propagation and measurement of ultrashort laser pulses were all included in this chapter. By the measurement techniques of ultrashort pulses, we restricted the discussion to the correlation techniques, which has been widely used because of its simplicity. It should be here clear to the reader, how the characterizations of ultrashort laser pulse can be measured. We also showed that for the purpose of pulse-asymmetry measurements, it is enough to use the third-order correlation.

In chapter 3, we described the principles and the experimental setup of a high-dynamic range third-order correlator using series of the two nonlinear crystals: the second-harmonic and third-harmonic generators. We mainly concentrated on the analysis of how to achieve a high-dynamic range. It was shown that there are two main problems to resolve: increasing the signal-to-noise ratio and the harmonic conversion efficiencies while the UPA must be maintained.

Chapter 4 showed the measured results and respective discussions. The characterized curve of the intensity attenuator shows a dynamic of about 3×10^2, which leads to a theoretically estimated dynamic range of about 10^{11}. The p-pulses problems introduced by the correlator were described and some appropriate solutions were also proposed and simulated with a computer program using Lab2. The high-dynamic range correlation measured with the SiC detector showed a dynamic range of about 10^7 or more, depending on the intensity of input laser pulse. It was suggested to use a more sensitive detector to realize higher dynamic range, such as a

PMT. The problem caused by ASE was also mentioned in this chapter.

Bibliography

[1] T. H. Maiman: "Stimulated Optical Radiation in Ruby", *Nature* **187**, 493 (1960).

[2] R. Menzel, *Photonics: Linear and Nonlinear Interactions of Laser Light and Matter*, Springer-Verlag, Berlin (2001).

[3] R. L. Fork, B. I. Greene, and C. V. Shank: "Generation of optical pulses shorter than 0.1 psec by colliding pulse mode-locking", *Appl. Phys. Lett.* **38**, 671 (1981).

[4] A. Baltuska, Z. Wei, M. S. Pshenichnikov, and D. A. Wiersma: "Optical pulse compression to 5fs at a 1-MHz repetition rate" *Opt. Lett.* **22**, 102 (1997).

[5] U. Morgner, F. X. Kärtner, S. H. Cho, Y. Chen, H. A. Haus, J. G. Fujimoto, E. P. Ippen, V. Scheuer, G. Angelow, and T. Tschudi: "Sub-two-cycle pulses from a Kerr-lens mode-locked Ti:sapphire laser", *Opt. Lett.* **24**, 411 (1999).

[6] P. Maine, D. Strickland, P. Bado, M. Pessot, and G. Mourou: "Generation of ultrahigh peak power pulses by chirped pulse amplification", *IEEE. J. Quantum Electron.* **24**, 398 (1988).

[7] R. F. Service: "Laser Labs Race for the Petawatt", *Science* **301**, 154 (2003).

[8] G. Petite, P. Agostini, and H. G. Muller: "Intensity dependence of non-perturbative above-threshold ionisation spectra: experimental study", *J. Phys. B: At. Mol. Phys.* **21**, 4097 (1988).

[9] L. A. Lompre, Anne L'Huillier, M. Ferray, P. Monot, G. Mainfray, and C. Manus: "High-order harmonic generation in xenon: intensity and propagation effects", *J. Opt. Soc. Am. B* **7**, 754 (1990).

[10] J. C. Kieffer, M. Chaker, J. Matte, H. Pepin, C. Cote, Y. Beaudoin, T. Johnston, C. Y. Chien, S. Coe, G. Mourou, and O. Peyrusse: "Ultrafast x-ray sources", *Phys. Fluids B* **5**, 2676 (1993).

[11] M. M. Murnane, H. C. Kapteyn, M. D. Rosen, and R. W. Falcone: "Ultrafast X-ray pulses from laser-produced plasmas", *Science* **251**, 531 (1991).

[12] K. W. D. Ledingham, P. McKenna, R. P. Singhal: "Applications for Nuclear Phenomena Generated by Ultra-Intense Lasers", *Science* **300**, 1107 (2003).

[13] I.D. Jung, F.X. Krtner, J. Henkmann, G. Zhang, U. Keller: "High-dynamic-range characterization of ultrashort pulses", *Appl. Phys. B* **65**, 307 (1997).

[14] A. Braun, J. V. Rudd, H. Cheng, G. Mourou, D. Kopf, I. D. Jung, K. J. Weingarten, U. Keller: "Characterization of short-pulse oscillators by means of a high-dynamic-range autocorrelation measurement", *Opt. Lett.* **20**, 1889 (1995).

[15] D. Giulietti, M. Galimberti, A. Giulietti, L. A. Gizzi, R. Numico, P. Tomassini, M. Borghesi, V. Malka, S. Fritzler, M. Pittman, K. Ta Phouc, and A. Pukhov: "Production of ultracollimated bunches of multi-MeV electrons by 35 fs laser pulses propagating in exploding-foil plasmas", *Phys. Plasmas* **9**, 3655 (2002).

[16] S.J. Moon, D.C. Eder: "Theoretical investigation of an ultrashort-pulse coherent x-ray source at 45 Å", *Phys. Rev. A* **57**, 1391 (1998).

[17] H. Daido: "Review of soft x-ray laser researches and developments", *Rep. Prog. Phys.* **65**, 1513 (2002).

[18] P. E. Young, M. E. Foord, J. H. Hammer, W. L. Kruer, M. Tabak, and S. C. Wilks : "Time-Dependent Channel Formation in a Laser-Produced Plasma", *Phys. Rev. Lett.* **75**, 1082 (1995).

[19] M. Borghesi, A. J. MacKinnon, L. Barringer, R. Gaillard, L. A. Gizzi, C. Meyer, O. Willi, A. Pukhov, and J. Meyer-ter-Vehn: "Relativistic Channeling of a Picosecond Laser Pulse in a Near-Critical Preformed Plasma", *Phys. Rev. Lett.* **78**, 879 (1997).

[20] G. Malka, J. C. Adam, F. Amiranoff, S. D. Baton, N. Blanchot, A. Héron, G. Laval, J. L. Miquel, P. Mora, H. Pépin1, and C. Rousseaux: "Dynamics of Subpicosecond Relativistic Laser Pulse Self-Channeling in an Underdense Preformed Plasma", *Phys. Rev. Lett.* **80**, 1658 (1998).

[21] S. Bastiani, A. Rousse, J. P. Geindre, P. Audebert, C. Quoix, G. Hamoniaux, A. Antonetti, and J. C. Gauthier: "Experimental study of the interaction of subpicosecond laser pulses with solid targets of vary initial scale lengths", *Phys. Rev. E* **56**, 7179 (1997).

[22] J. Collier, D. Hitchcock, C. Danson, and K. Weingarten: "Pulse contrast measurements of the VULCAN CPA front end Oscillators", *CLF Annual Report* **1996/97**, 190.

[23] M. A. Duguay, J. W. Hansen: "An ultrafast ligh gate", *Appl. Phys. Lett.* **15**, 192 (1969).

[24] D. H. Auston: "Measurement of picosecond pulse shape and background level", *Appl. Phys. Lett.* **18**, 249 (1971).

[25] S. Luan, M. H. R. Hutchinson, R. A. Smith, and F. Zhou, "High dynamic range third-order correlation measurement of picosecond laser pulse shapes," *Meas. Sci. Technol.* **4**, 1426 (1993).

[26] A. C. Tien, M. Nantel, G. Mourou, D. Kaplan, M. Bouvier: "High-dynamic-range laser-pulse-contrast measurement with a plasma-shuttered streak camera", *Opt. Lett.* **22**, 1559 (1997).

[27] P. F. Moulton: "Spectroscopic and laser characteristics of Ti:Al_2O_3," *J. Opt. Soc. Am. B* **3**, 125 (1986).

[28] C. Rullière (Ed.), *Femtosecond Laser Pulses: Principles and Experiments*, Springer, Berlin (1998).

[29] W. K. Kuo, Y. T. Huang, and S. L. Huang: "Three-dimensional electric-fieldvector measurement with an electro-optic sensing technique" *Opt. Lett.* **24**, 1546 (1999).

[30] J. D. Jackson, *Classical Electrodynamics*, John Wiley & Sons, Inc., New York (1998).

[31] R. W. Boyd, *Nonlinear Optics*, Academic Press, New York (2003).

[32] Y. R. Shen, *The Principles of Nonlinear Optics*, John Wiley, New York (1984).

[33] I. N. Bronstein, K. A. Semendjajew, G. Musiol, H. Mhlig, *Taschenbuch der Mathematik*, Harri Deutsch (1993).

[34] F. Schwabl, *Quantenmechanik*, Springer, Berlin (1993).

[35] J. C. Diels, W. Rudolph, *Ultrashort Laser Pulse Phenomena: Fundamentals, Techniques, and Applications on a Femtosecond Time Scale*, Academic Press, California (1996).

[36] P. A. Franken, A. E. Hill, C. W. Peters, and G. Weinreich: "Generation of Optical Harmonics", *Phys. Rev. Lett.* **7**, 118 (1961).

[37] R. L. Sutherland, *Handbook of Nonlinear Optics*, Marcel Dekker Inc., New York (2003).

[38] J. A. Armstrong, N. Bloembergen, J. Ducuing, and P. S. Pershan: "Interactions between Light Waves in a Nonlinear Dielectric", *Phys. Rev.* **127**, 1918 (1962).

[39] S. A. Akhmanov, V. A. Vysloukh, and A. S. Chirkin, *Optics of Femtosecond Laser Pulses*, American Institute of Physics, New York (1992).

[40] J. E. Midwinter and J. Warner: "The effects of phase matching method and of uniaxial crystal symmetry on the polar distribution of second-order non-linear optical polarization", *Brit. J. Appl. Phys.* **16**, 1135 (1965).

[41] R. Sauerbrey: "Nichtlineare Optik", *Optional lecture* **SS/2004**, FSU Jena-Germany (2004).

[42] W. Knoechner, *Solid-State Laser Engineering*, Springer, Berlin (1999).

[43] E. I. Blount and J. R. Klauder: Recovery of Laser Intensity from Correlation Data, *J. Appl. Phys.* **40**, 2874 (1969).

[44] M. Bass, *Handbook of Optics: Fundamentals, Techniques, and Design*, Volume **I**, McGraw-Hill, Inc. (1995).

[45] D. Meshulach, Y. Barad, and Y. Silberberg: "Measurement of ultrashort optical pulses by third-harmonic generation," *J. Opt. Soc. Am. B* **14**, 2122, (1997).

[46] K. Naganuma, K. Mogi and H. Yamada: "General Method for Ultrashort light pulse chirp measurement", *IEEE. J. Quantum Electron.* **25**, 1225 (1989).

[47] J. -C. Diels, J. J. Fontaine, I. C. McMichael, and F. Simoni: "Control and measurement of ultrashort pulse shapes (in amplitude and phase) with femtosecond accuracy", *Appl. Opt.* **24**, 1270 (1985).

[48] R. Trebino, K. W Delong, D. N. Fittinghoff, J. N. Sweetser, M. A. Krumbgel, and B. A. Richman: "Measuring ultrashort laser pulses in the time-frequency domain using freuqency-resolved optical gating", *Rev. Sci. Instrum.* **68**, 3277 (1997).

[49] C. Iaconis and I. A. Walmsley: "Spectral phase interferometry for direct electric-field reconstruction of ultrashort optical pulses", *Opt. Lett.* **23**, 792 (1998).

[50] J. W. Nicholson, J. Jasapara, W. Rudolph, F. G. Omenetto, and A. J. Taylor: "Full-characterization of femtosecond pulses by spectrum and cross-correlation measurements", *Opt. Lett.* **24**, 1774 (1999).

[51] P. Langlois and E. P. Ippen: "Measurement of pulse asymmetry by three-photon-absorption autocorrelation in a GaAsP photodiode", *Opt. Lett.* **24**, 1868 (1999).

[52] P. O'Shea, M. Kimmel, X. Gu, and Rick Trebino: "Increased-bandwidth in ultrashort-pulse measurement using an angle-dithered nonlinear-optical crystal," *Opt. Exp.* **7**, 342 (2000).

[53] C. Spielmann, L. Xu, and F. Krauz: "Measurement of interferometric autocorrelations: comment," *Appl. Opt.* **36**, 2523 (1997).

[54] M. Hacker: "Neue Möglichkeiten und Anwendungen der Phasenmodulation ultrakurzer Laserimpulse", *DISS.* **2003-24**, available in Zweigbibliothek Physik, Jena - Germany (2003).

[55] G. Stobrawa: "Aufbau und Anwendung eines hochauflösenden Impulsformers zur Kontrolle ultrakurzer Laserimpulse", *DISS.* **2003-27**, available in Zweigbibliothek Physik, Jena - Germany (2003).

[56] B.Schmidt, M.Hacker, G.Stobrawa, and T.Feurer: "LAB2-A virtual femtosecond laser lab", *http://www.lab2.de*

[57] M. Aoyama, A. Sagisaka, S. Matsuoka, Y. Akahane, F. Nakano, K. Yamakawa: "Contrast and phase characterization of a high-peak-power 20-fs laser pulse", *Appl. Phys. B* **70**, 149 (2000).

Declaration

Ich erkläre, daß ich die vorliegende Arbeit selbständig verfaßt und keine anderen als die angegebenen Quellen und Hilfsmittel benutzt habe.

Jena, den 11.09.2004

Nguyen Xuan Truong

Acknowledgement

The work for this thesis was carried out in the Institute of Optics and Quantum electronics, FSU Jena - Germany. On this occasion, I would like to express my deep gratitude to all colleagues and students of FSU Jena and Institute of Optics and Quantum electronics, who have supported me with numerous encouragements, suggestions, and corrections, in the work as well as in my life. Please permit me not to thank by name all of you here - though I wish to do so. It will surely take much of your time to find my thanks to each of you. All I would like to say is that just your friendly smiles - anywhere and anytime - have always made me find Physics more and more fascinating. In particular, I am greatly indebted to Prof. R. Sauerbrey for providing me the opportunity to study in the scientific environment of Jena, for giving the thesis' theme, for the very interesting questions in his lectures of physics, and for his so kind secretaries. Special thanks go to PD Dr. H. G. Walther for his supports, encouragements and sympathy during the time I have been in Jena. I am grateful also to my thesis supervisors: Dr. M. Harker, Dr. G. Strobrawa, and R. Netz, for teaching the experimental skills, for exciting discussions and for their kindnesses.

I would like also to express my appreciation to those who directly gave me supports in the work. To Prof. K. W. D. Ledingham, Dr. A. Nazakin, Dr. I. Uschmann, Dr. A. Morak, and Dr. H. G. Walther for reading and correcting the manuscript. To W. Ziegler and F. Ronnerberger for all technical helps and for the essential softwares. To Mrs. B. Beleites for introducing the third-order correlator in Lab I and for the measurement data. To X-ray group, for their cooperation and friendly working environment. To Dr. L. Veisz for his remote-guidance.

Last but never the least, I am very grateful to my parents, who always believe me and advise me not "working too hard". To my sister, brother and my relatives for their tolerance during the time we had been together and for taking care of my parents while I am not at home. Finally, to my Dear - for her love and belief!

Jena, August 2004.

Nguyen Xuan Truong